INSTITUTO TECNOLOGICO Y DE ESTUDIOS
SUPERIORES DE MONTERREY
CAMPUS MONTERREY
DIVISION DE INGENIERIA
PROGRAMA DE GRADUADOS EN INGENIERIA

TECNOLÓGICO
DE MONTERREY

EXPERIMENTAL AND SIMULATED AIR BENDING STUDY ASSISTED BY DIGITAL IMAGE RECOGNITION

PRESENTADA COMO REQUISITO PARCIAL PARA
OBTENER EL GRADO ACADEMICO DE
MAESTRO EN CIENCIAS CON ESPECIALIDAD
EN SISTEMAS DE MANUFACTURA

POR
DAVID ALEJANDRO CONTRERAS GARZA

MONTERREY, N. L. DICIEMBRE 2010

INSTITUTO TECNOLOGICO Y DE ESTUDIOS
SUPERIORES DE MONTERREY

CAMPUS MONTERREY

DIVISION DE INGENIERIA

PROGRAMA DE GRADUADOS EN INGENIERIA

TECNOLÓGICO
DE MONTERREY

EXPERIMENTAL AND SIMULATED AIR BENDING STUDY ASSISTED BY DIGITAL IMAGE RECOGNITION

PRESENTADA COMO REQUISITO PARCIAL PARA
OBTENER EL GRADO ACADEMICO DE

**MAESTRO EN CIENCIAS CON ESPECIALIDAD
EN SISTEMAS DE MANUFACTURA**

POR

DAVID ALEJANDRO CONTRERAS GARZA

MONTERREY, N. L. **DICIEMBRE 2010**

INSTITUTO TECNOLÓGICO Y DE ESTUDIOS SUPERIORES DE MONTERREY

CAMPUS MONTERREY

DIVISIÓN DE INGENIERÍA

PROGRAMA DE GRADUADOS EN INGENIERÍA

Experimental and Simulated Air Bending Study Assisted by Digital Image Recognition

PRESENTADA COMO REQUISITO PARCIAL PARA OBTENER EL GRADO ACADÉMICO DE

MAESTRO EN CIENCIAS CON ESPECIALIDAD EN SISTEMAS DE MANUFACTURA

POR:

DAVID ALEJANDRO CONTRERAS GARZA

MONTERREY, N.L. DICIEMBRE 2010

ABSTRACT

Advanced High Strength Steels (AHSS) are being used in industry for their strength and low weight, but to manufacture them and form them correctly there is a need to predict the final geometry. Air bending generates a non-perfect geometry by nature, so there is a need for alternate ways of measurement.

Image recognition software is widely used for biomedical and biometrics applications. It has proven to automatically measure and characterize different aspects of an image in a reliable way.

The proposed methodology of this study is to predict the final geometry of an air bending test and compare it with an image recognition algorithm so that the differences are detected automatically and faster than current methods.

DEDICATORY

A mi familia

por brindarme su apoyo y cariño en todo momento

ACKNOWLEDGMENTS

This thesis couldn't be possible without the guidance, help and opportune advise of many highly qualified professors. First I want to thank my gratitude to Dr. Nicolas Hendrichs, who's advise, vision and trust were vital to the completion of this thesis.

I am very grateful to Dr. Ciro Rodriguez and Dr. Héctor Siller for their support on the critical moments of the completion of this thesis. Their experience and knowledge helped this thesis to achieve its final shape. I also would like to thank to Dr. Alex Elías for his consistency in support throughout this program. And to all the institution's teachers who have shown passion and dedication in the search for knowledge and know how to transmit that passion.

In addition I want to show my appreciation for all the people who assisted in the experimentation: Gabriel Soto, Froylán Mier, José Obedt Figueroa, Rogelio Pérez, Lorenzo Bianchetti and José Guadalupe Corona whose help and expertise made all the measurements and simulations possible. Also my partners and friends who always lent a helping hand when needed and moral support for the difficult times Araceli Rivera, Beatriz Montoya, Omar Fernandez and Arturo Marbán.

And to all my friends outside the institution who have shown interest and offered a helping hand whenever needed and to my girlfriend Mary who supported me in many different ways with this thesis, showed me the advantages of post-graduate studies and have shared with me some wonderful moments.

To the memory of Jorge Mercado and Javier Arredondo

Table of Contents

List of Figures

List of Tables

List of Tables

1 Introduction

1.1 Application description

Sheet metal is one of the fundamental forms used in metalworking, it is metal formed into thin and flat pieces that can be bent and cut into different shapes. Sheet bending is an important manufacturing process because it changes the general shape of the sheet into a more volumetric purpose by plastically deforming the material and changing its shape.

There are different methods commonly used for sheet bending, such as folding (a), air bending (b), rotary bending (c), flange bending (d) shown in Figure 1 (Marciniak, 2002). Each of these bends features different characteristics in the final product like; curve profile, residual stress, thickness and geometry. (Kalpakjian, 2003)

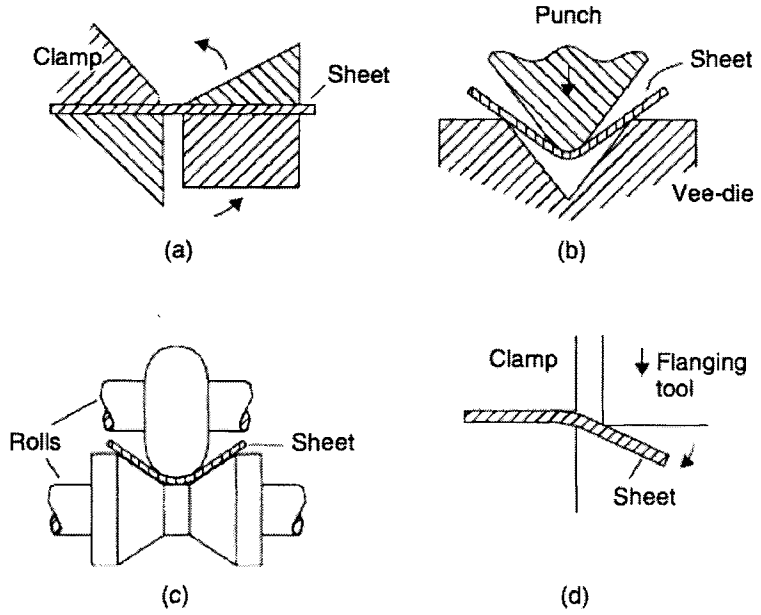

Figure 1. Different process of forming sheet-metal (Marciniak, 2002)

From the different methods to achieve the desired bend one of the modern methods is air bend, which doesn't require a different bottom die for each bending angle. Nonetheless it requires a deep understanding of the phenomena occurring in the material to get the desired angle and radius.

There are some empiric rules for air bend, which can be applied for common engineering materials but for advanced high strength steel (AHSS) these rules are not a good enough predictor. Because of this we need to take certain measures to ensure that simulations are similar to test results.

1.2 Research focus

The primary reason behind the use of AHSS in automobiles is the reduction of fuel consumption and the safety of occupants as (Koppel Conway, 2009) mentions. Also manufacturers hope to reduce their manufacturing costs.

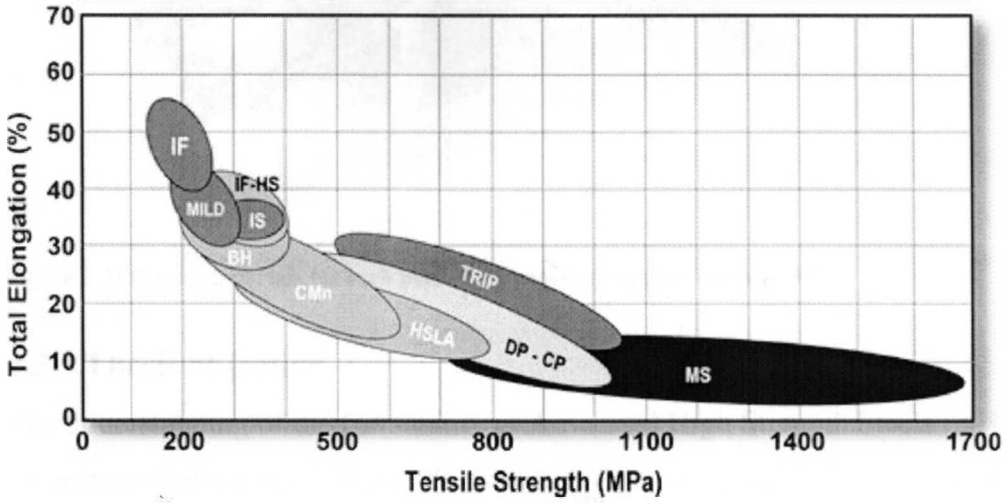

Figure 2. Different materials in tensile strength vs elongation (IISI, 2006)

Due to their superior mechanical properties, crashworthiness and mass avoidance there has been and increase in demands for AHSS in the automotive industries (Hudgins, 2010). However because of their low formability their implementation has not been widely adopted yet. According to Figure 2 the current AHSS materials have low elongation and high tensile stress.

There are some vital parts that are manufactured to date according to (Koppel Conway, 2009) because they make a difference in crash test in terms of security but require some special treatments. Once deformed an AHSS should be replaced, it should not be heated or hammered to recuperate it's original shape after a crash. The vital parts that are made from high strength are shown in Figure 3.

The springback deformation becomes a critical problem when experienced in AHSS (Keler, 1994). There industry has a need to predict springback correctly to overcome manufacturing problems.

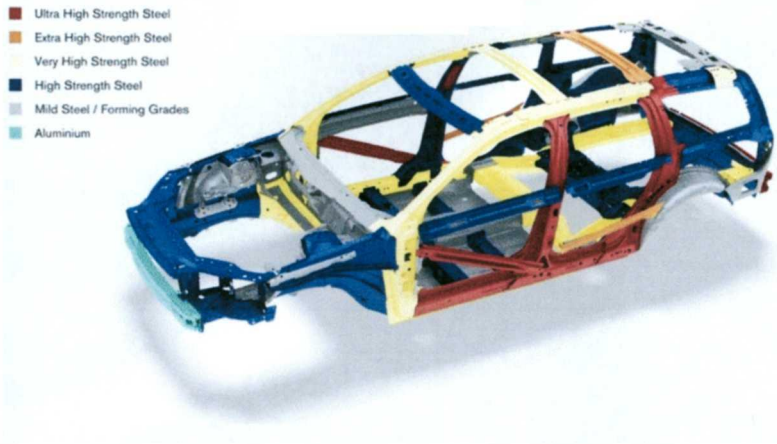

Figure 3. Different materials for each part of the chassis (Koppel Conway, 2009)

1.3 Thesis objective

The understanding of the formability of Advanced High Strength Steels (AHSS) is one of its greatest limitations as this is the first step to achieve better results while forming these materials. (Singuang Xu, 2005)

The objective of this thesis is to test these materials with different rolling directions and calculate the effect of these directions on spring-back. Using image recognition software to asses the differences of the real shapes with their idealized desired counterparts. It will be used to describe automatically the general shape and dimension of each test and each simulation. The reason for this is that air bending produces non-ideal results compared to straight lines and circular bending zones as shown in Figure 4.

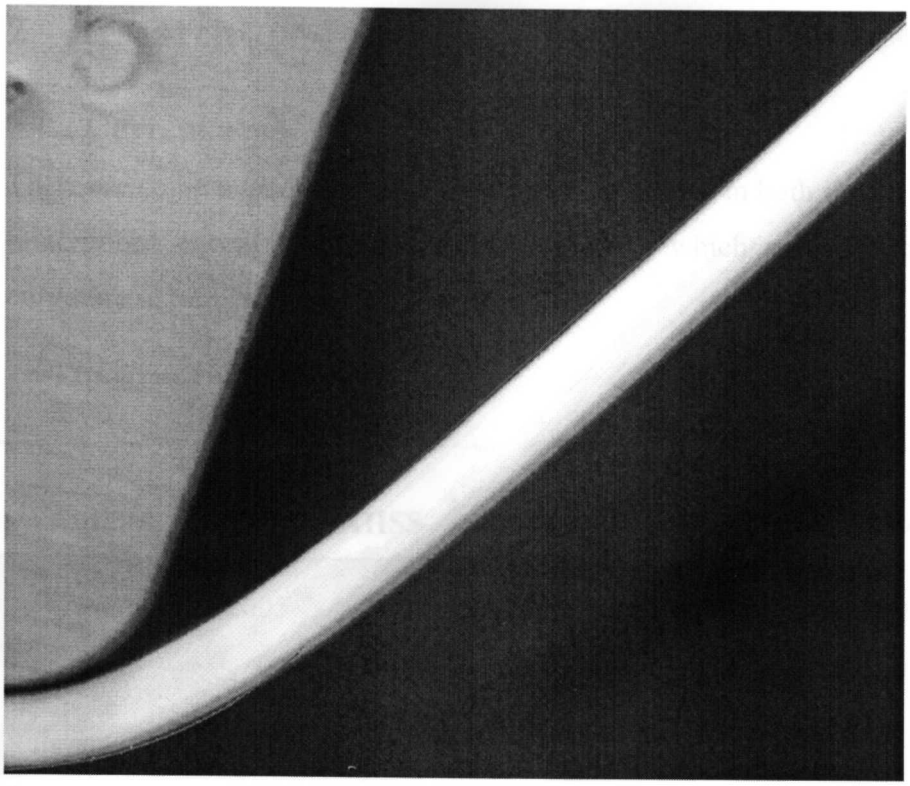

Figure 4. The red line is a perfect circle or line, the image shows the non-linearity and non-circularity of a real air bending test.

2 Research

2.1 Current work

There are some experiments and algorithms developed in both fields, but there is no clear integrations except from (Garcia-Romeu, 2005) which presents an algorithm for the curvature in air bending.

Table 1. Current work in air bending

Author	Year	AHSS	Experiment	Simulation	Anisotropy	Geom. prediction
GARCIA-ROMEU	2005		¶	¶	¶	¶
Nguyen	2004		¶	¶	¶	
Rahmani	2008		¶	¶	¶	
Current work	2010	¶	¶	¶	¶	¶

Table 2. Current work in measurement air bending

Author	Year	Automated	Multiple images	For Air Bending	Regression for desired geometry
GARCIA-ROMEU	2005	¶		¶	
Chueng	2009	¶	¶		
Fallahi	2010	¶			
Current work	2010	¶	¶	¶	¶

2.2 Anisotropy

A material with the same properties in any direction is called isotropic, but most industrial sheet will show a difference in properties measured in test-pieces aligned in

various directions. This variation is known as planar anisotropy. In a tensile test of an isotropic material it is expected that the width and thickness strains would be equal; if not, some anisotropy exists. (Marciniak, 2002)

Thin sheets are often very anisotropic because of their production history according to literature (Gil Sevillano, 2003). This is this reason they display planar anisotropy or orthotropy.

The first option to describe their anisotropic planar behavior is the Hill's (1948) orthotropic extension to the Von Mises yield criterion it's used in (Rahmani, 2009) to describe the differences in a stress strain curve as Figure 5.

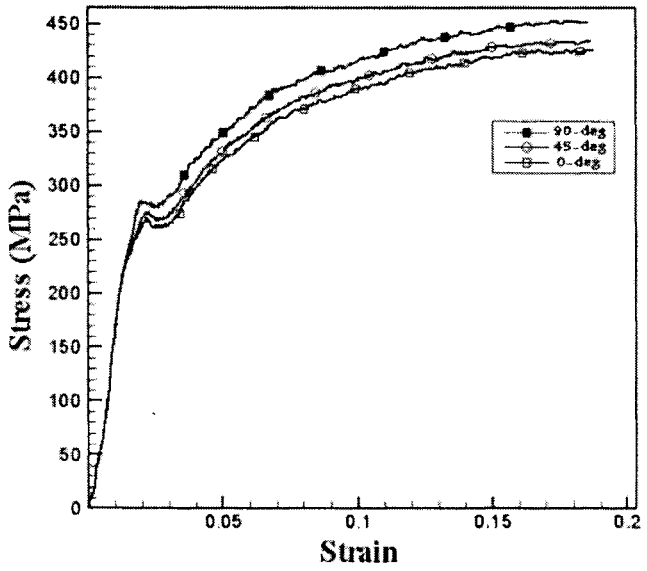

Figure 5. Different orientations for Stress Strain curve (Rahmani, 2009)

In materials in which the properties depend on direction, the state of anisotropy is usually indicated by an R-value as shown in Equation 1.

Equation 1

$$R = \frac{\ln \frac{w}{w_0}}{\ln \frac{w_0 l_0}{w l}}$$

As a first option to describe the anisotropic behavior the Hill's (1948) orthotropic extension to the Von Mises yield criterion can be used. The Equation 2 shows the basic principle of the Hills criterion. (Marciniak, 2002)

Equation 2

$$F(\sigma_{22}-\sigma_{33})^2 + G(\sigma_{33}-\sigma_{11})^2 + H(\sigma_{11}-\sigma_{22})^2 + 2\left(L\sigma_{23}^2 + M\sigma_{31}^2 + N\sigma_{12}^2\right) - 1 = 0$$

To make the respective measurements it is needed to perform a tensile or compressive test in the sheet plane and in the through-thickness direction, which is a difficult task if not impossible. It is possible to show that the trough-thickness strength is equal to the balanced biaxial in-plane tensile tests. Some laboratories can do that using hydrostatic bulging testing device (which isn't the available for this experiment)

The need for an additional test can be avoided by an exploitation of the in-plane tensile test. Lankford (1950) said that the contraction of the cross-section of an in-plane tensile specimen contains the same information provided by the hydrostatic bulging test. (Gil Sevillano, 2003)

Equation 3

$$R = \left.\frac{d\varepsilon_2^p}{d\varepsilon_3^p}\right|_{d\varepsilon_1^p} = \left[2\left(\frac{Z}{X}\right)^2 - 1\right]$$

The effect of R on the yield surface is show in Figure 6.

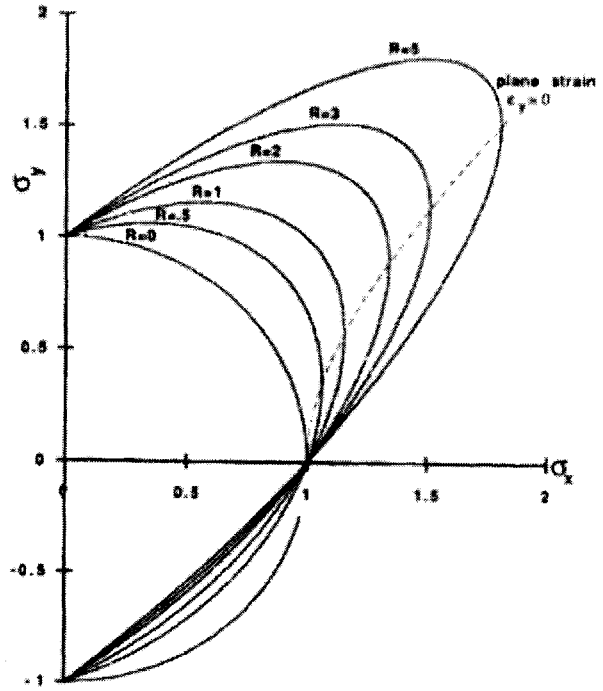

Figure 6. Effects of anisotropy index (R) in the 2D yield surface. (Gil Sevillano, 2003)

This R is known as the anisotropy index.

2.3 Hardening

To achieve the desired spring-back movement it is required some kind of hardening after the yield surface is surpassed. (Simo, 1998) A typical deformation with no hardening is shown in Figure 7 and what we are trying to achieve an idealized deformation state like Figure 8.

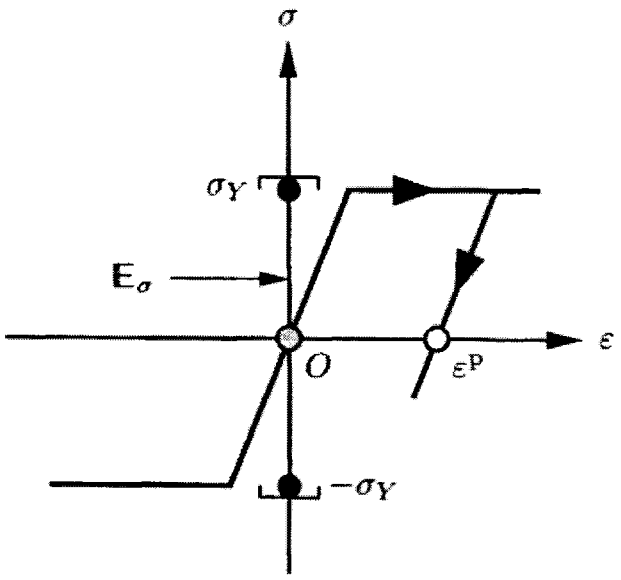

Figure 7. Typical stress-strain curve without hardening (Simo, 1998)

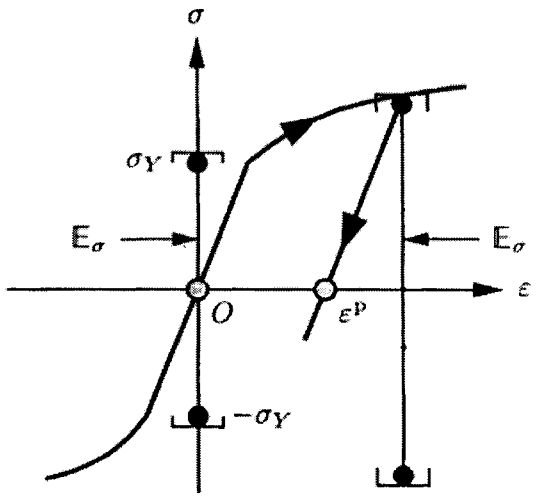

Figure 8. Typical stress-strain curve with isotropic hardening (Simo, 1998)

There are two kinds of hardening that can be taken into account, the isotropic and kinematic. The isotropic hardening is ideal for hardenings that are in just one direction, as the material deforms the hardening happen in all directions as shown in Figure 9. Kinematic hardening is the simplest form that can take into account the Bauschinger effect (which describes how a material hardens in one direction and softens in the other). It is postulated that the hardening is produced by a pure translation of the yield surface in

the stress space without any change in size or shape as shown in Figure 10. (Chakrabarty, 2010) According to (Simo, 1998) the kinematic hardening is preferred to applications of fatigue or applications where there is one load in one side and then another load in the opposite direction.

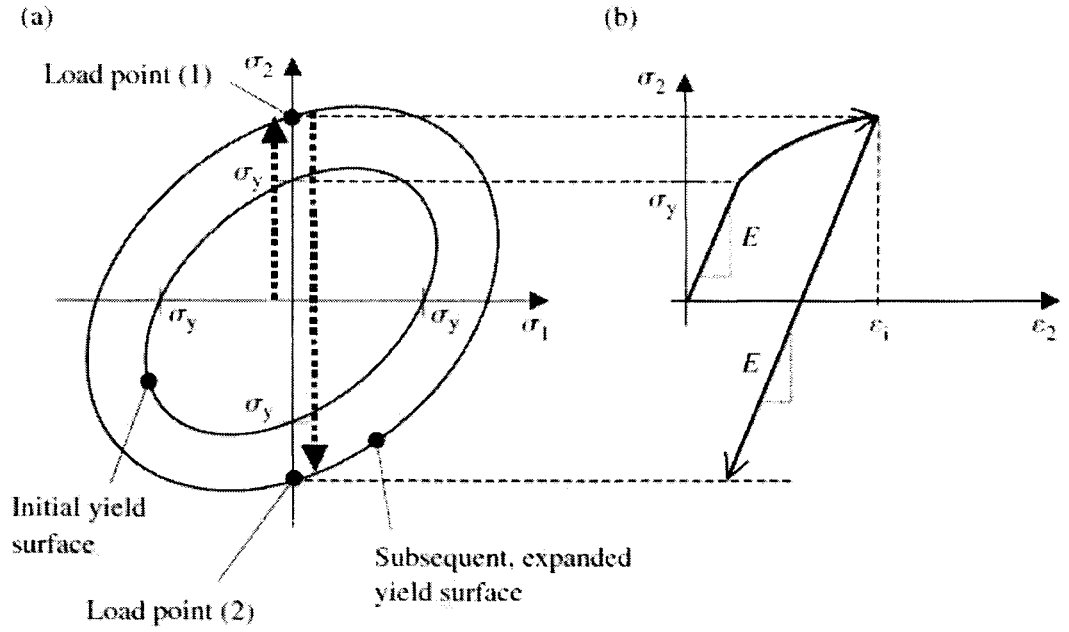

Figure 9. Isotropic hardening, which affects every direction (Dunne, 2005)

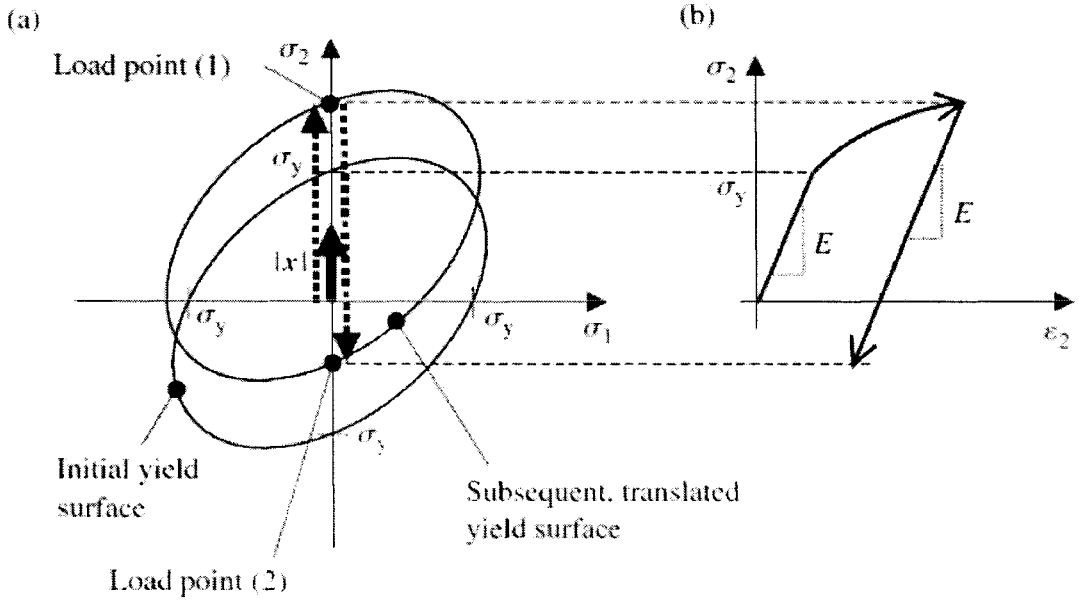

Figure 10. Kinematic hardening, which displaces the yield surface in the stress direction (Dunne, 2005)

2.4 Image recognition

Image recognition is widely used in biometric and biomedical applications, thus there are some implemented algorithms that recognize, measures and modifies certain aspects of an image. Thus for the air bending some similar implications may occur and are used during the development of the algorithm.

After each bend the desired geometry is a sheet with a final bend angle (after spring-back) and a bend radius, assuming a circular profile in the bend (Kalpakjian, 2003). This is not normally the case for air bend, thus a special application of image recognition software is used to generally describe the final geometry.

One of the ways to acquire a digital image good enough for image recognition software is a digital camera (Lin, 2010). The image can later be treated to acquire the desired characteristics of contrast that will be transformed to numbers in a matrix, either in a black and white image or a gray scale.

According to (Garcia-Romeu, 2005), to obtain a digital image of an object, with enough contrast to be detected by image recognition software, it is needed to paint white the face of the object that will be subject to analyzing. Also there must be a black opaque surface in the background. Testing that way a maximum contrast is achieved.

When there is a need to detect morphology it is recommended to use binary images (Russ, 1995). That way the background characteristics are separated completely from the object characteristics. Also it is needed to clean defects like dust, or cracks and there are different methods to filter them by adding, subtracting or eliminating automatically fractions of the image (González, 2009).

To process the image there are some proven general methodologies as (Reza Fallahi, 2010), where it is needed an image with certain characteristics as a contrast ratio, color gamut or general size in pixels. Then there is a region of that image that is being analyzed. The required feature is extracted and after that measured or classified.

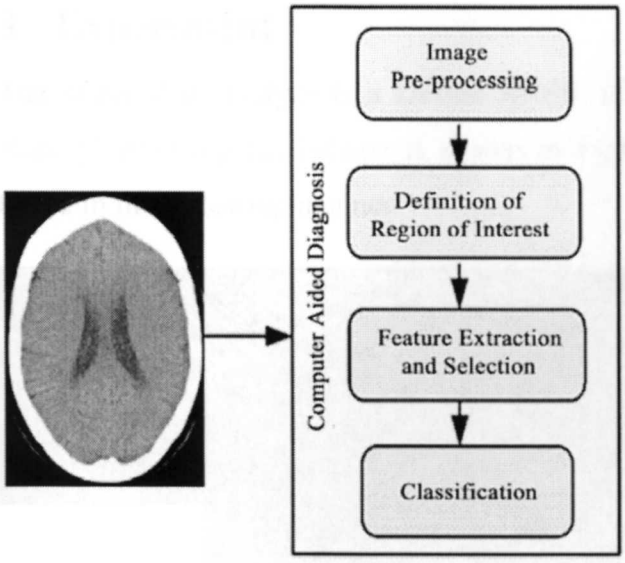

Figure 11. Processing of a brain CT scan (Reza Fallahi, 2010)

2.4.1 Skinning image

Once a single white object is achieved the software can analyze different aspects of the image, in this case being the bend angle, and the radius. To get the bend angle the software first makes the image so tin it's only 1px thick. This process is known as thinning and is used to characterize general geometry as if it were thin branches as shown in Figure 12.

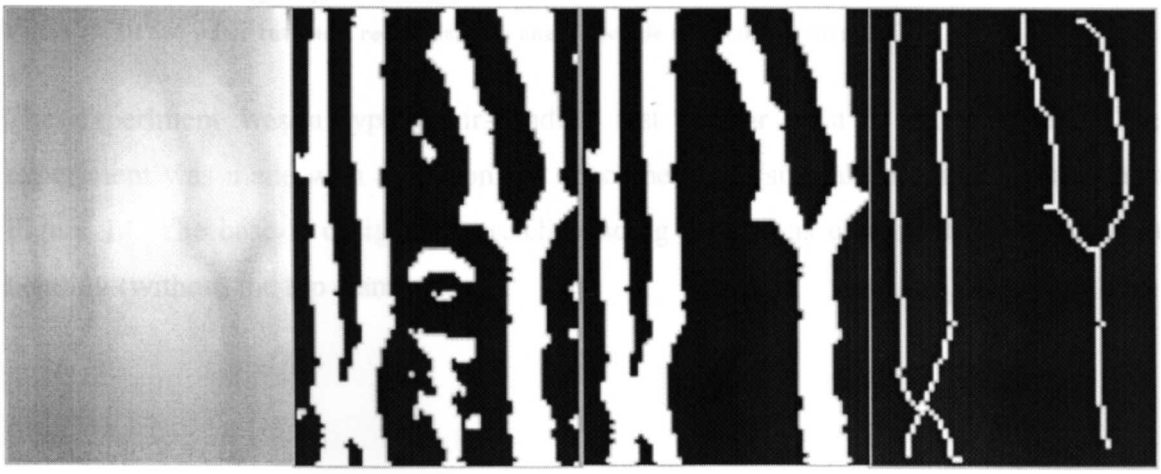

Figure 12. Black & white, filtering and thinning steps for finger-vein image recognition (Cheng-Bo, 2009)

3 Experiment

The material to analyze is a DP600 AHSS, this material was water cut to avoid heat affected zone the final shape is shown in Figure 13. The material was measured and tested in the following manner.

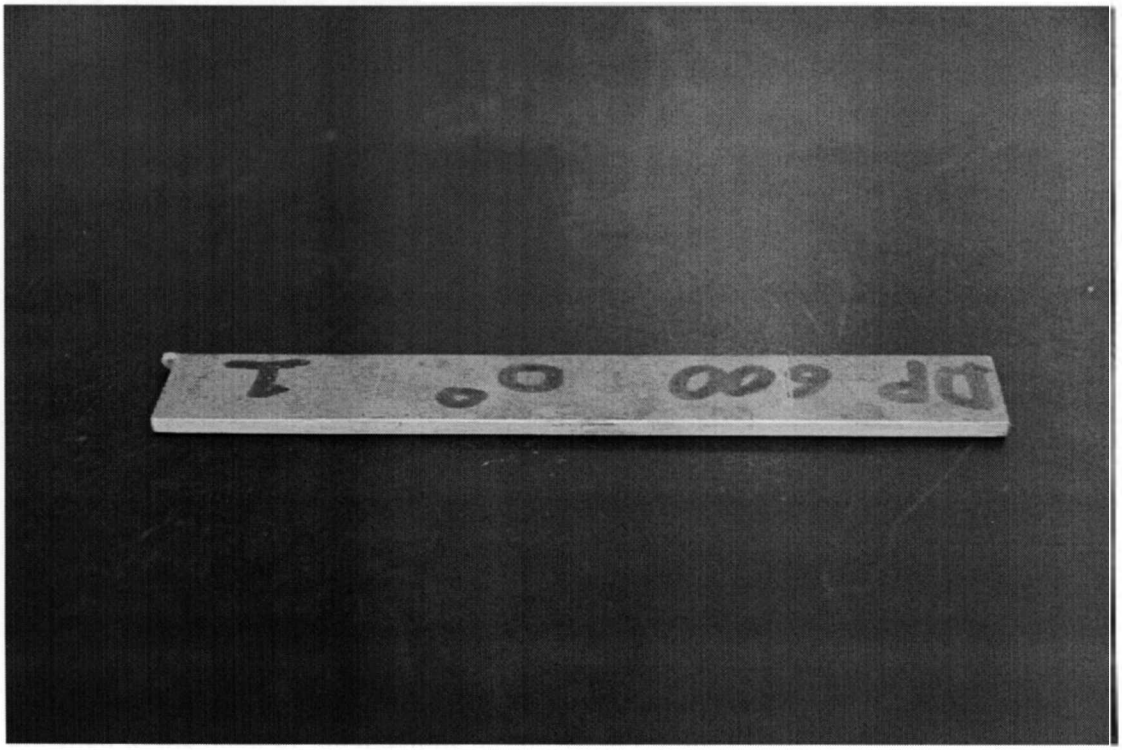

Figure 13. DP600 water cut into a rectangle, with one white side to enhance contrast

The experiment was a typical air-bending test similar to a 3 point bending. The experiment was made with a tension test machine and a special holding base shown in Figure 14. The base is design for stretch bending but it was used in these case for air bending (without the top clamps).

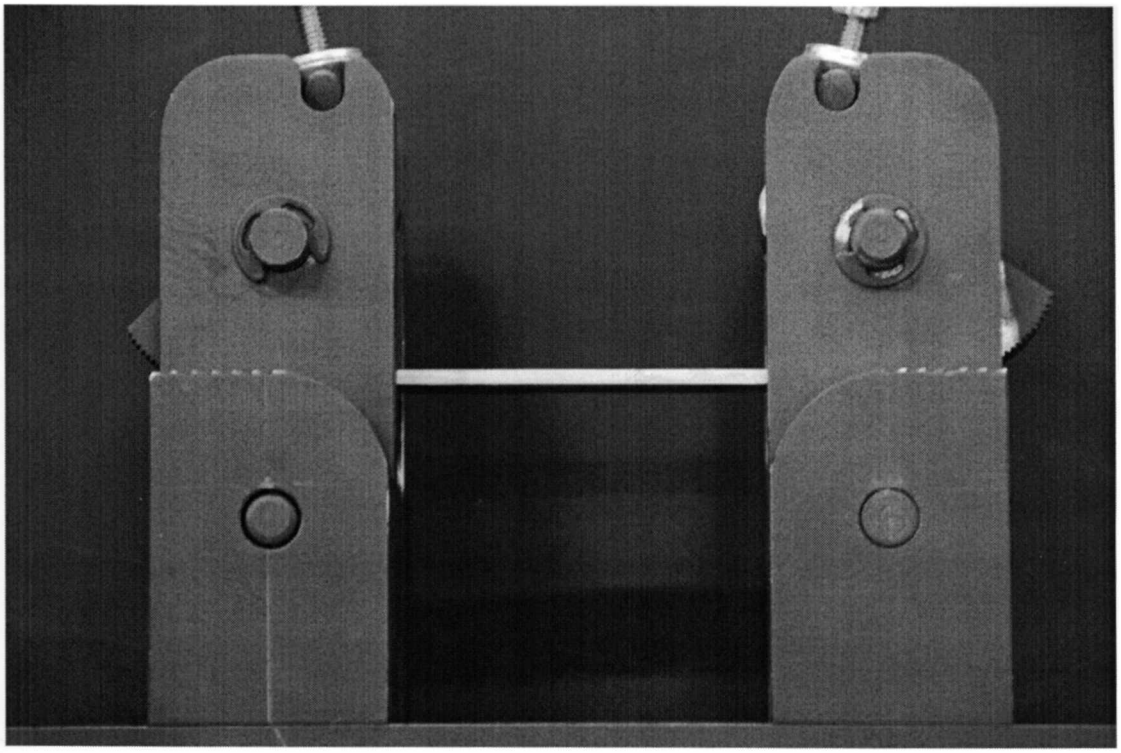

Figure 14. Base for air bending, shows the white side of the sample piece.

The test specimen was painted in color white on one side to get a better contrast for the posterior measurements. Also to enhance the contrast an opaque black surface was attached to the back of the machine as shown in Figure 15.

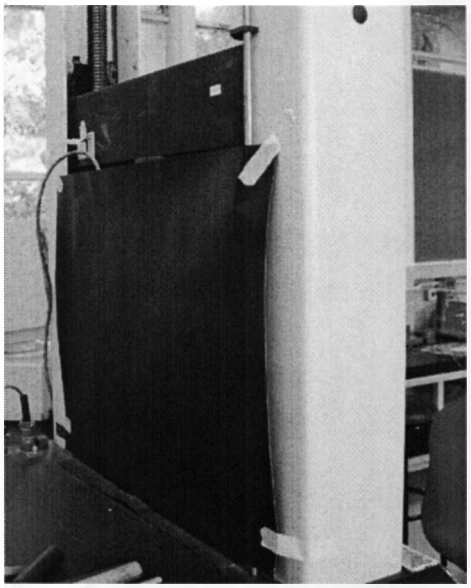

Figure 15. Black opaque cover in the back of the machine to enhance contrast

The air bending was concluded after an approximate initial angle of 90°. After that the reaction forces were measured with the load cell and computer shown in Figure 17 and Figure 16.

Figure 16. The control unit for the air bend test

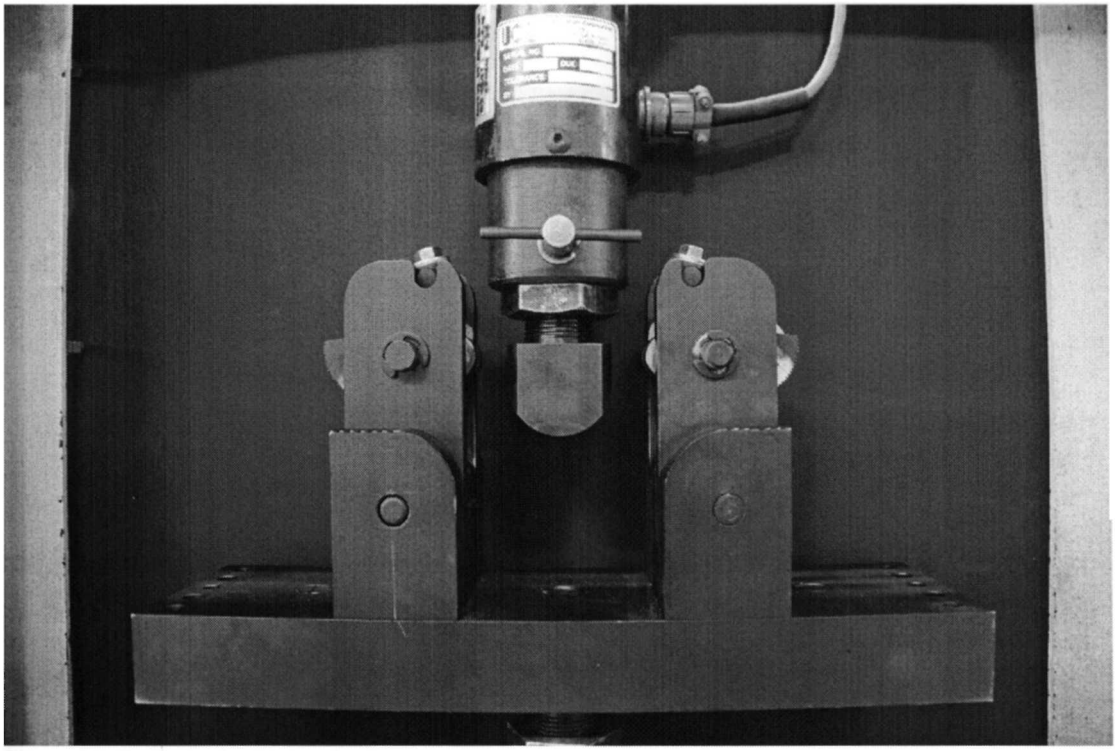

Figure 17. Load cell with one of the punches

Two pictures were taken during the test. The first one is taken after the desired angle was achieved as shown in

Figure 18. and the second one after removing the load as shown in Figure 19

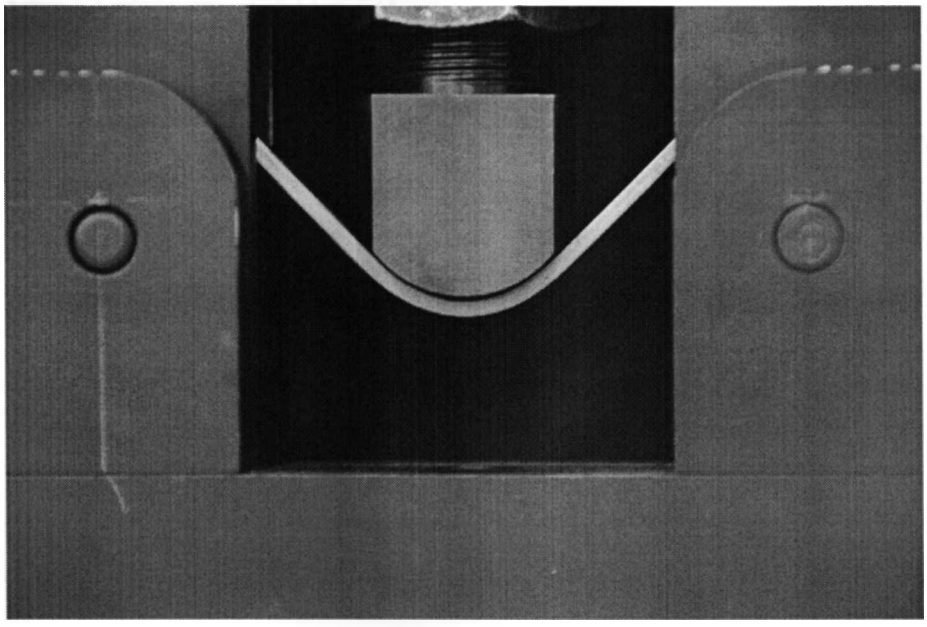

Figure 18. Test sample before springback

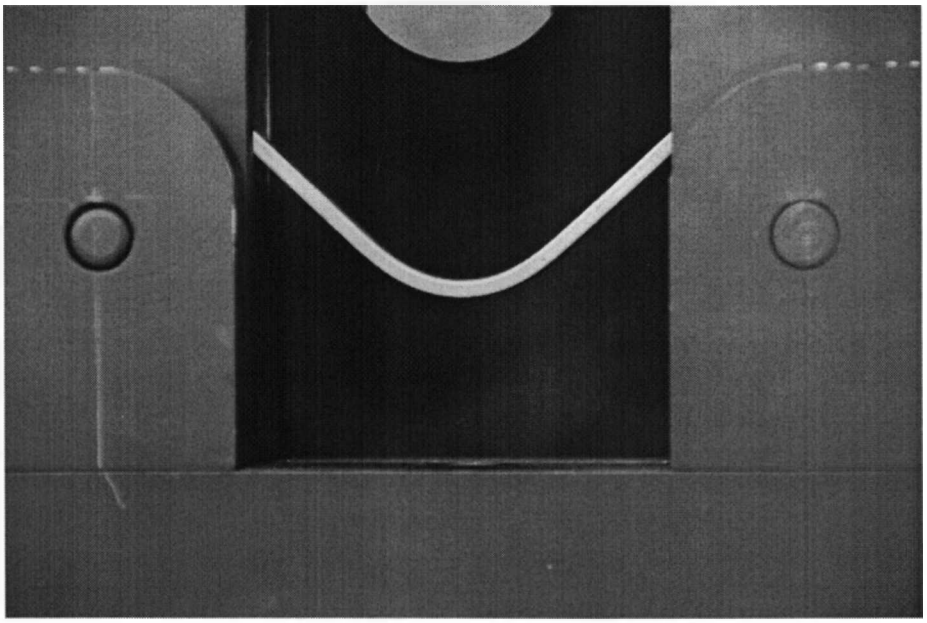

Figure 19. Test sample after springback

The pictures were taken with a Nikon D200 camera with 10.2 MP with general specs on Table 3, with a tripod to stabilize the image and a lens of 11.1x and used to full capacity to achieve a less distorted flat image so the angles are not distorted.

Table 3. Camera and picture specifications

Dimensions	3872x2592
Brand	NIKON CORPORATION
Model	NIKON D200
Color	RGB
Color Profile	sRGB IEC61966-2.1
Focal Length	200
Alpha channel	NO
F-number	5.6
Exposure time	¼
File Size	3.7 MB
Format	JPG

The test specimens were air bent by different punches shown in Table 4

Table 4. Material for each die radius and rolling direction angle

Die [mm]	0°	45°	90°
7.5	DP600	DP600	DP600
12	DP600	DP600	DP600
15	DP600	DP600	DP600
22.5	DP600	DP600	DP600

The general setup of the test is shown in Figure 20 were there is the United tension test machine, with the special base for air bending, a background black panel and the control system to measure forces and displacements.

Figure 20. General setup for the test

3.1 Digital image analysis algorithm

This approach describes an algorithm that analyzes a digital image to obtain an approximation of the bend radius and bend angle with Matlab.

To achieve a sample with enough contrast for the algorithm to work, one side of the piece has to be white in a black background (Garcia-Romeu, 2005). The pieces need to be painted whit a white water based paint that doesn't add thickness to the faces of the samples.

From this image the program asks for the user to input a rectangle that encloses approximately the bending zone. That information is used to separate both straight lines so that it can acquire both angles and rotate the image so it's more symmetric.

To measure the bend radius it is needed to acquire the borders of the image, it wasn't possible to acquire the mid-surface proposed by (Kalpakjian, 2003) in the bending zone because of the limitations of Matlab. The internal and external radius were used to achieve the same effect.

Given a list of data, it may be needed to find the line that "best" fits this data set. The "least squares method" determines that fit (Cheung, 2005). When the best fit for this data is not a line but a different function then a non-linear regression is required.

Once the border are obtained those are transformed into coordinates to insert into a non-linear regression, based on the equation of a perfect circle. The non-linear regression minimizes the squared error and returns the radius in pixels. (Seber, 2003)

The pixels need to be changed into units by comparing a portion of the image with a real measurement; this is achieved form the left side of the image.

3.2 Simulation

The simulation was performed used a simulation software especial for forming operations and large displacements called DEFORM. The simulation setup is shown in figure were a simplified version of the holding tool is shown in Figure 21. The simulation was made with the measurements of the punch stroke taken in the experiment to try to achieve the same bending angles.

The simulation didn't require any boundary conditions because in air bending the work piece has to slip into the die.

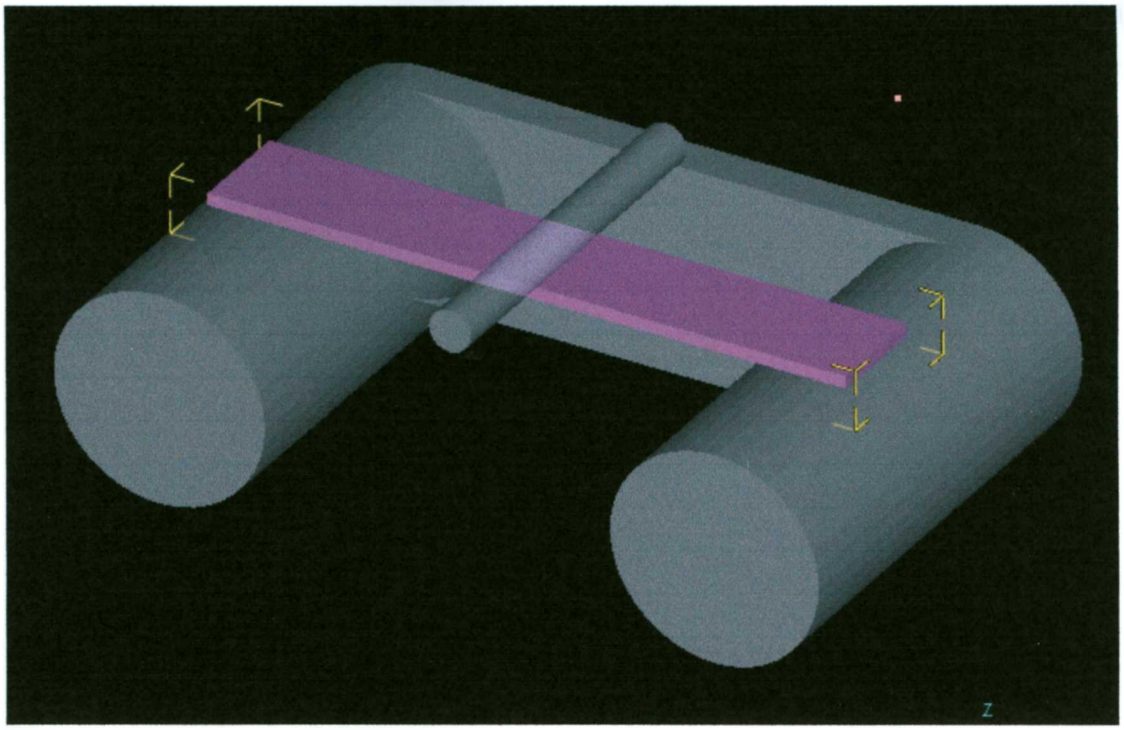

Figure 21. Geometry for simulation

To optimize the mesh the contact zone has a much denser mesh than the other parts of the work piece as shown in Figure 22. This approach helped to reduce the time consumed during each simulation.

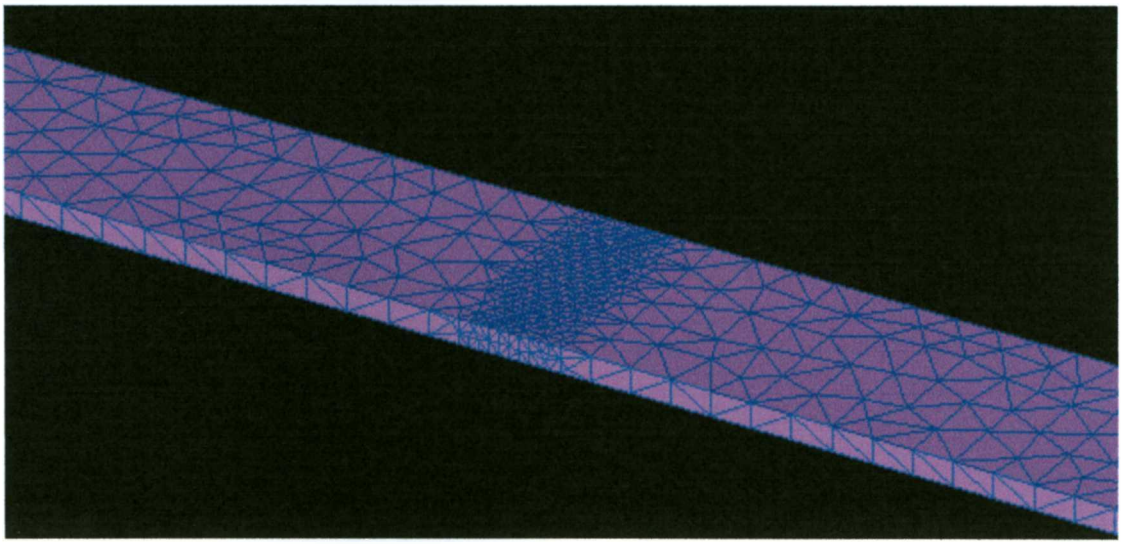

Figure 22. Finer mesh in the bending zone

The data supplied to DEFORM was taken from the thesis of (Corona, 2010), from the material DP600. It was supplied as a Flow stress curve as shown in Figure 23. The anisotropy index are shown in Figure 24 and the modulus of elasticity is 135,255 N/mm^2

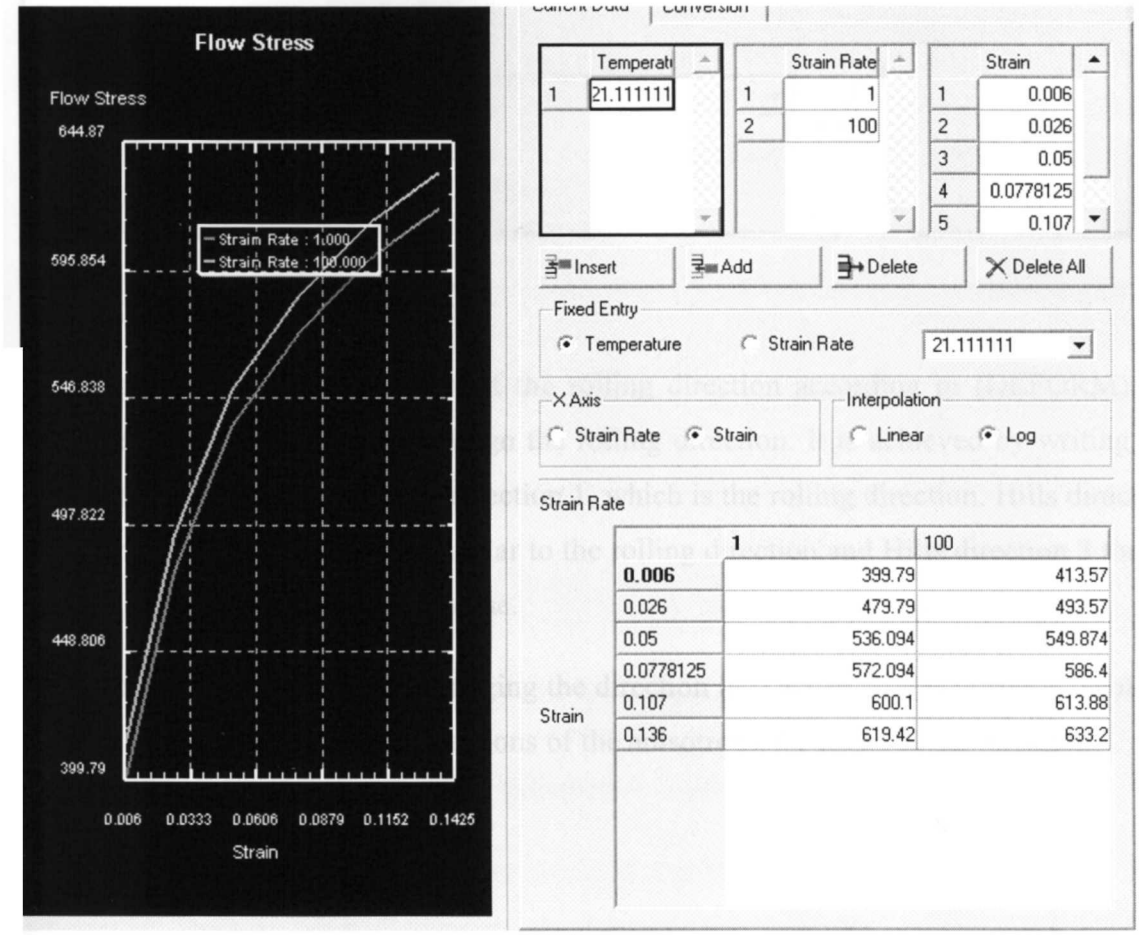

Figure 23. Graph for the Flow Stress for DP600

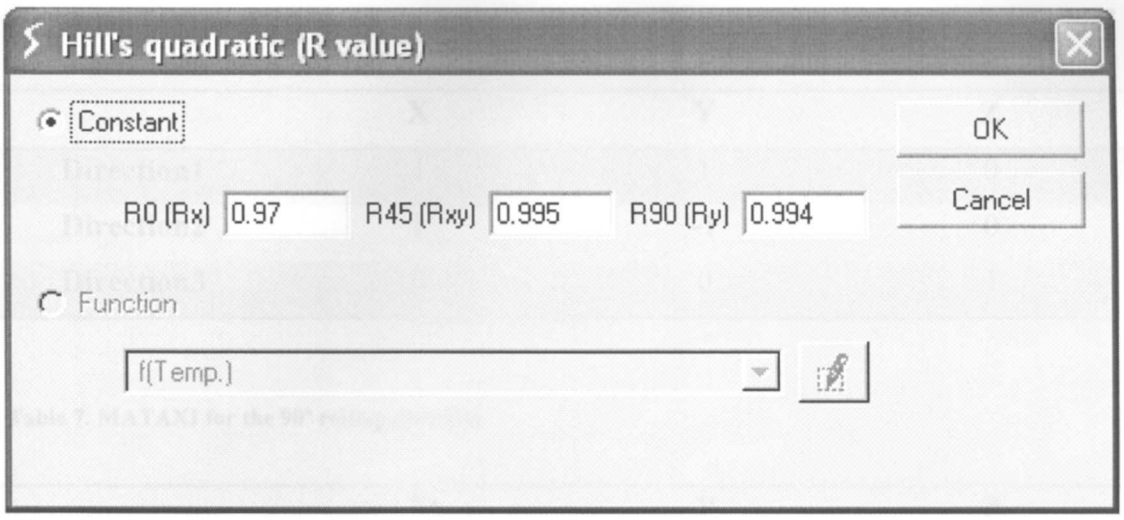

Figure 24. Anisotropy index for DP600

To assign the correct orientation of the rolling direction according to (DEFORM) we used the function MATAXI to assign the rolling direction. It is achieved by writing the directions of a vector in de Hills direction 1, which is the rolling direction, Hills direction 2, which is the direction perpendicular to the rolling direction and Hills direction 3 that is perpendicular to the sheet metal plane.

Changing the code as text and changing the direction in it achieved this purpose. Table 5, Table 6 and Table 7 show the directions of the anisotropy for each rolling direction.

Table 5. MATAXI for the 0° rolling direction

	X	Y	Z
Direction1	1	0	0
Direction2	0	1	0
Direction3	0	0	1

Table 6. MATAXI for the 45° rolling direction

	X	Y	Z
Direction1	1	1	0
Direction2	1	-1	0
Direction3	0	0	1

Table 7. MATAXI for the 90° rolling direction

	X	Y	Z
Direction1	0	1	0
Direction2	1	0	0
Direction3	0	0	1

4 Results

4.1 Image recognition results

A convergence analysis was made to test if and when the process stabilizes the result and how much pixels are needed to get a satisfactory outcome.

For an expected radius of 1, it was obtained that the most important indicator is the amount of pixels in the bent zone, as observed in Figure 25 and Figure 26 from 200 px and beyond it shows stable results.

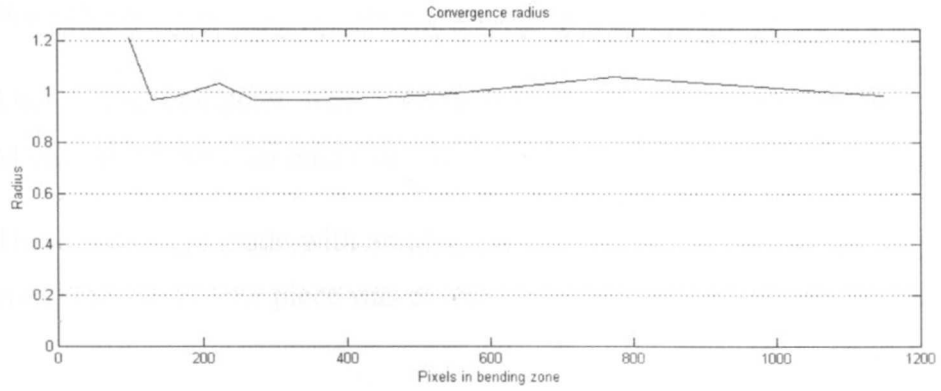

Table 6. MATAXI for the 45° rolling direction

	X	Y	Z
Direction1	1	1	0
Direction2	1	-1	0
Direction3	0	0	1

Table 7. MATAXI for the 90° rolling direction

	X	Y	Z
Direction1	0	1	0
Direction2	1	0	0
Direction3	0	0	1

4 Results

4.1 Image recognition results

A convergence analysis was made to test if and when the process stabilizes the result and how much pixels are needed to get a satisfactory outcome.

For an expected radius of 1, it was obtained that the most important indicator is the amount of pixels in the bent zone, as observed in Figure 25 and Figure 26 from 200 px and beyond it shows stable results.

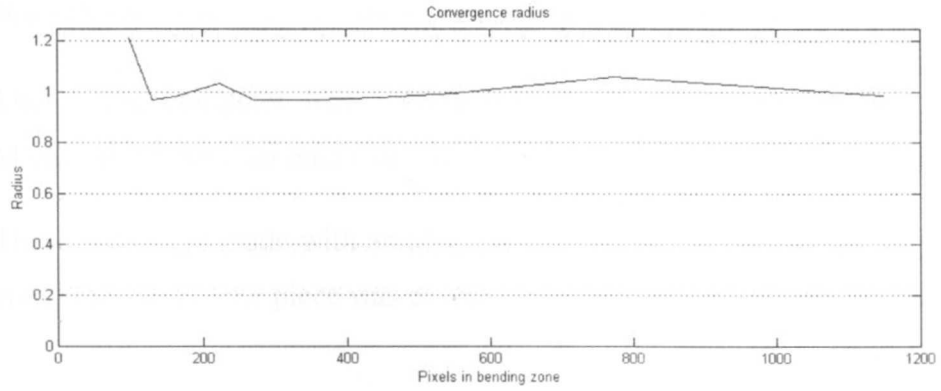

Figure 25. Radius measurement stabilizes after 200px in the bending zone

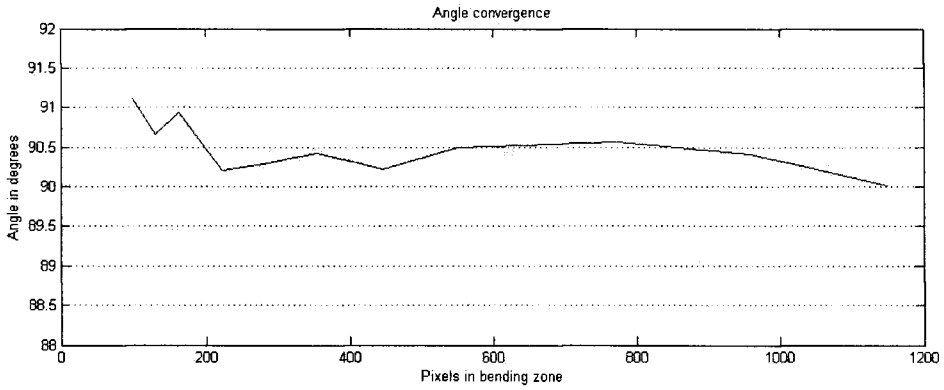

Figure 26. Angle measurement stabilizes after 200px in the bending zone

This test was made to limit the size of the image so the analysis is faster with good enough results. If the size of the image is too large the time taken to process it increases exponentially as shown in Figure 27.

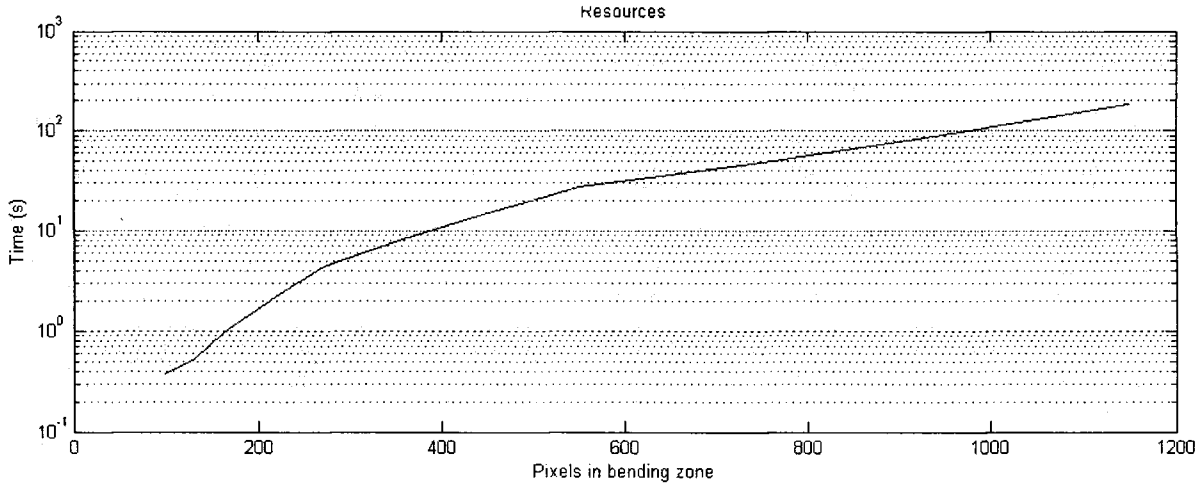

Figure 27. Time taken by the algorithm to process data compared to the number of pixels

The testing computer was a Virtual Machine running in Parallels Desktop 4, with Microsoft XP SP3, an Intel Core2Duo 2.26 GHz, 512 MB RAM.

These tests were made with an ideal piece, designed in Solid Edge to have perfect shape and dimensions. The piece was exactly 1mm thick, 1mm internal radius and a bend angle

of 90°. The algorithm approximated the piece as shown in Figure 28. Where it shows a black line with the algorithm piece and a color line with the real idealized piece.

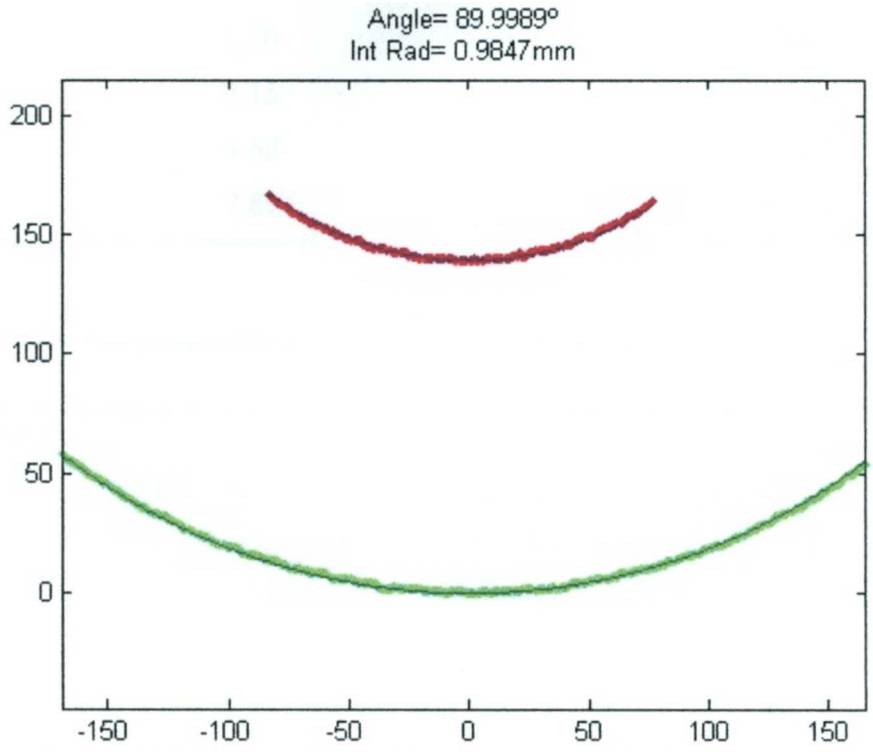

Figure 28. Internal and external radius (color) compared with the non linear regression (black)

For this ideal test the error is 0.001% for the angle and 1.53% for the radius.

The algorithm was also tested with real pieces. The results for radius and bend angle are shown in Table 8 and Table 9, they were compared to a measurement taken by a coordinate machine by taking only 4 points in the bending zone and 3 points for the straight lines compared to hundreds of pixels taken with a scanner.

Table 8. Comparison of the physical vs algorithm values of the radius

Radius			
Thickness	Physical	Algorithm	% Error
1.20	10.53	9.85	6.45
2.15	6.57	6.08	6.53
4.68	7.65	8.03	4.95
7.89	29.85	30.57	2.42

Table 9. Comparison of the physical vs algorithm values of the angle

Angle			
Thickness	Physical	Algorithm	% Error
1.20	119.54	119.43	0.09
2.15	102.69	104.40	1.66
4.68	119.91	120.32	0.34
7.89	89.77	89.74	0.04

4.2 Experiment results

Both the real test and the simulation resulted in a deformed piece after spring back, both were measured by the same standards. The image recognition software was used for all the experiments and also there were measurements of the Forces vs displacements.

4.2.1 Force

The tension test machine gives an accurate measurement of the force and displacement. The Figure 29 shows the data acquired during said experimentation.

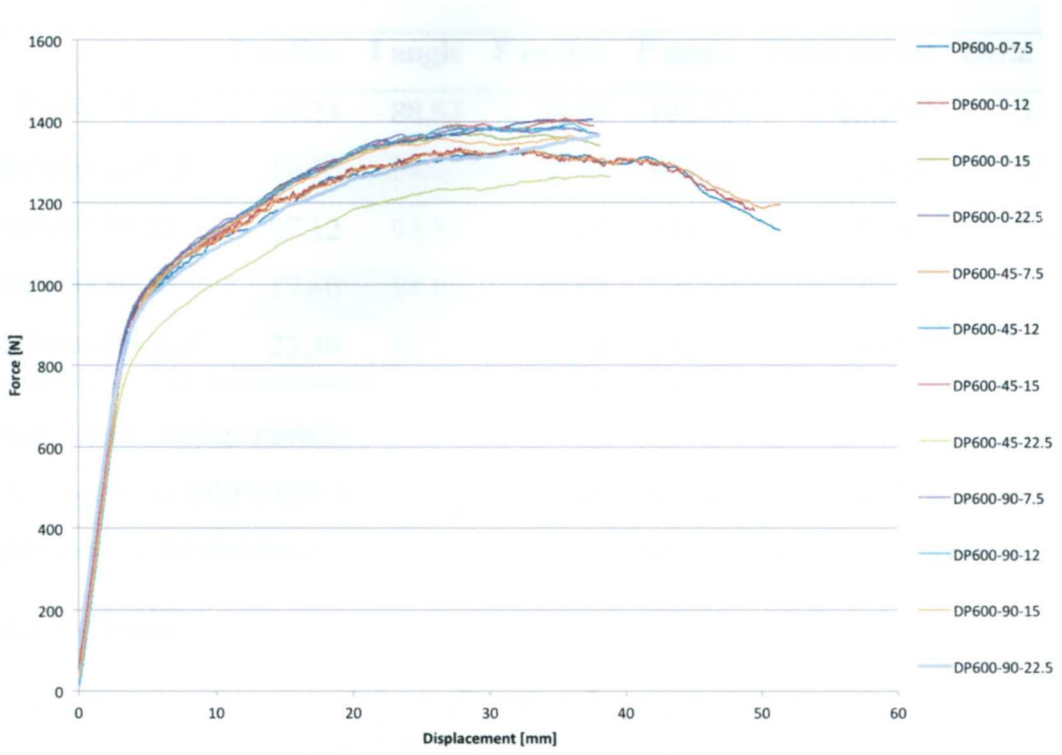

Figure 29. Force vs displacement in the experiment

4.2.2 Shape

The pictures were analyzed into the image recognition algorithm to detect the angle and radius before and after spring-back. The data is shown in Table 10.

Table 10. Measurements of the initial and final, angle and radius of the experiment

	I radius	I angle	F radius	F angle	Delta radius	Delta angle
DP600-0-7.5	14.58	85.37	15.29	96.31	4.87%	12.81%
DP600-0-12	16.54	87.63	16.68	98.44	0.85%	12.34%
DP600-0-15	21.46	90.04	20.04	100.71	-6.62%	11.85%
DP600-0-22.5	21.68	90.11	28.64	101.34	32.10%	12.46%
DP600-45-7.5	18.20	84.61	17.98	96.08	-1.21%	13.56%
DP600-45-12	17.16	91.92	21.80	103.09	27.04%	12.15%
DP600-45-15	17.72	95.13	21.43	105.23	20.94%	10.62%

	I radius	I angle	F radius	F angle	Delta radius	Delta angle
DP600-45-22.5	34.23	88.52	23.19	101.23	-32.25%	14.36%
DP600-90-7.5	19.30	94.96	18.75	105.52	-2.85%	11.12%
DP600-90-12	17.12	93.17	17.24	103.70	0.70%	11.30%
DP600-90-15	17.88	94.68	18.63	104.68	4.19%	10.56%
DP600-90-22.5	23.36	89.57	24.42	101.30	4.54%	13.10%

4.3 Simulation results

The software DEFORM has the option to analyze the forces and displacements of the punch after the test is concluded. The Figure 30 shows a graph of these tests.

4.3.1 Force

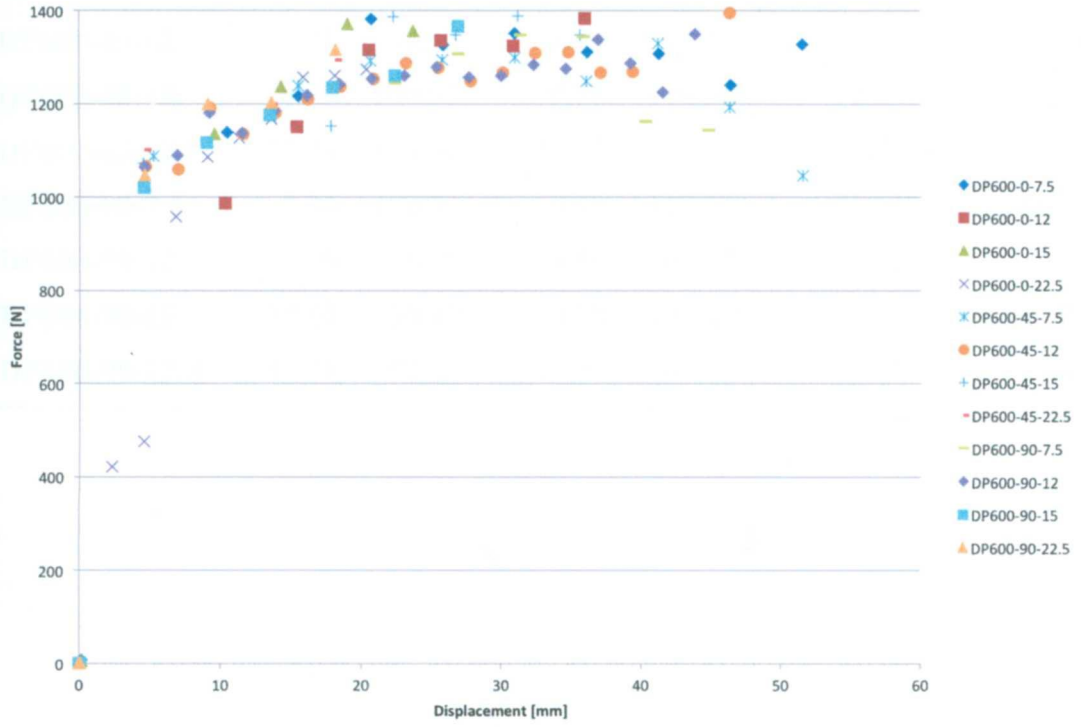

Figure 30. Force vs displacement in the simulation

4.3.2 Shape

The pictures taken form the display of DEFORM were analyzed into the image recognition algorithm to detect the angle and radius before and after springback. The data is shown in Table 11.

Table 11. Measurements of the initial and final, angle and radius of the experiment

	I radius	I angle	F radius	F angle	Delta radius	Delta angle
DP600-0-7.5	7.44	96.53	7.74	96.28	4.05%	-0.26%
DP600-0-12	7.12	98.13	7.68	106.39	7.85%	8.42%
DP600-0-15	10.40	96.57	10.17	99.63	-2.20%	3.17%
DP600-0-22.5	9.97	106.85	10.60	111.76	6.30%	4.59%
DP600-45-7.5	7.00	92.03	7.78	98.77	11.16%	7.32%
DP600-45-12	8.91	97.39	8.80	95.76	-1.26%	-1.68%
DP600-45-15	8.93	100.08	9.77	109.62	9.34%	9.54%
DP600-45-22.5	11.74	100.07	12.65	101.74	7.79%	1.67%
DP600-90-7.5	7.76	100.92	9.39	112.23	21.01%	11.21%
DP600-90-12	9.29	98.39	9.56	102.52	2.92%	4.20%
DP600-90-15	10.01	99.49	10.08	107.44	0.74%	7.99%
DP600-90-22.5	13.18	97.25	13.27	100.79	0.66%	3.64%

5 Discussion

There issues concerned the present work: the image recognition algorithm, the experimentation and the simulation.

5.1 Image recognition software

The algorithm designed for this particular case accomplished its purpose. As shown in Figure 25 the algorithm is fast and reliable when the image has at least 200px in the radius. The non-linear regression has shown to be precise in its prediction of the circular geometry as shown in Figure 28 the nonlinear regression mirrors the bending zone. Some fine-tuning may be needed to reduce that 1% error that may be due to the conversion of mm to pixels.

When confronted with experimental samples the algorithm did an acceptable job as shown in Table 8. The algorithm takes hundreds of points to make the calculations while the technician at the coordinate measuring machine took only 5 or 6. If fine-tuned and correctly used, it can give fast and reliable results for any amount of tests.

5.2 Air bending experimentation

The experiment worked as expected, the pieces presented springback and deformed a small percentage of their initial angle (around 12%). The forces the machine registered were all about the same for the different direction and punches. None of the materials fractured under said loads and punch radius. There were not clear effects of the different rolling directions on the forces applied, but with some more replicas the fine differences might be shown.

5.2.1 Air bending simulation

The simulation results had similar in forces, with maximum forces around 1,400 N. The models presented springback after the applied force. This springback was measured then with the image recognition algorithm. The bend angles and radiuses acquired with the algorithm had some differences with the desired values. The differences in Table 10 and Table 11 are noticeable and further refinement needs to be done.

5.3 General discussion

The experiments and the simulation were similar, the results in force prove to be about the same magnitudes for the simulation and experimentation Figure 31.

If the different punch radius are analyzed it seems that the initial mesh worked best for the 7.5mm punch than the others, however the general magnitudes are still acceptable compared with the experimental force measurements.

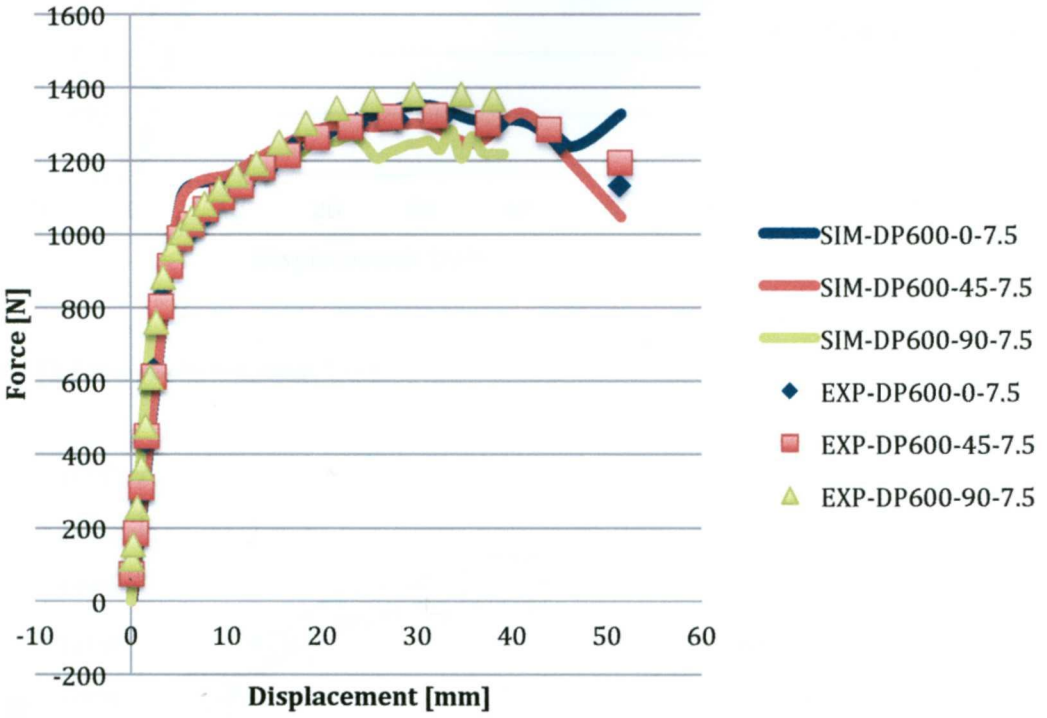

Figure 31. Force results for punch 7.5mm

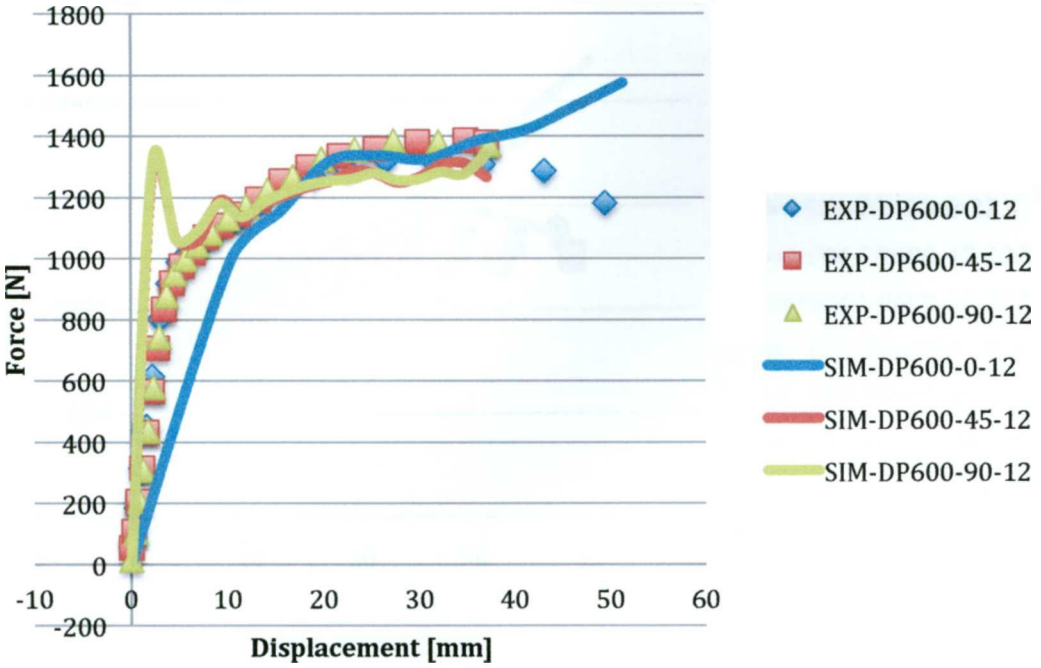

Figure 32. Force results for punch 12mm

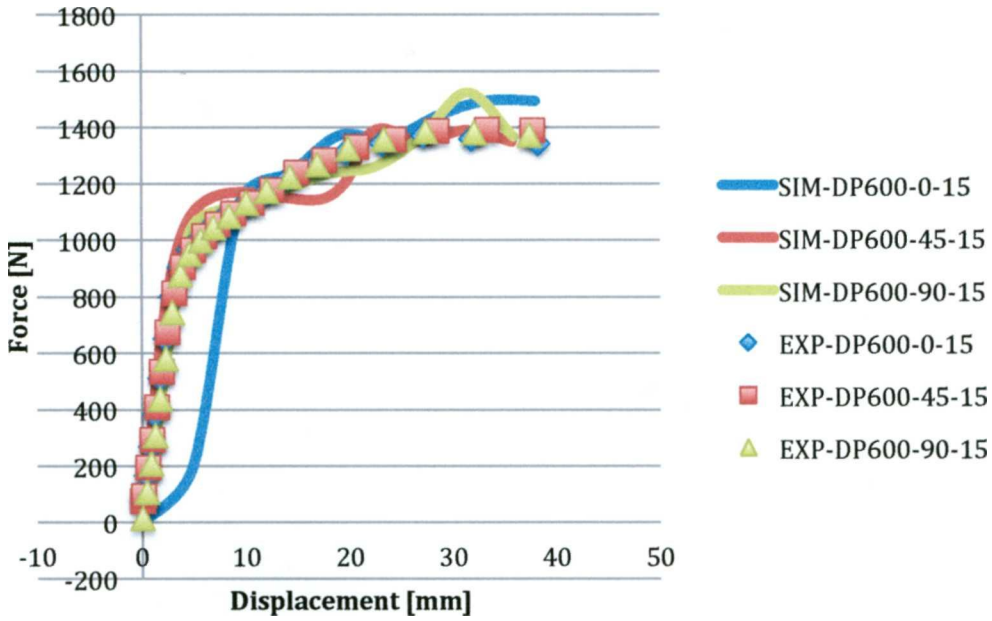

Figure 33. Force results for punch 15mm

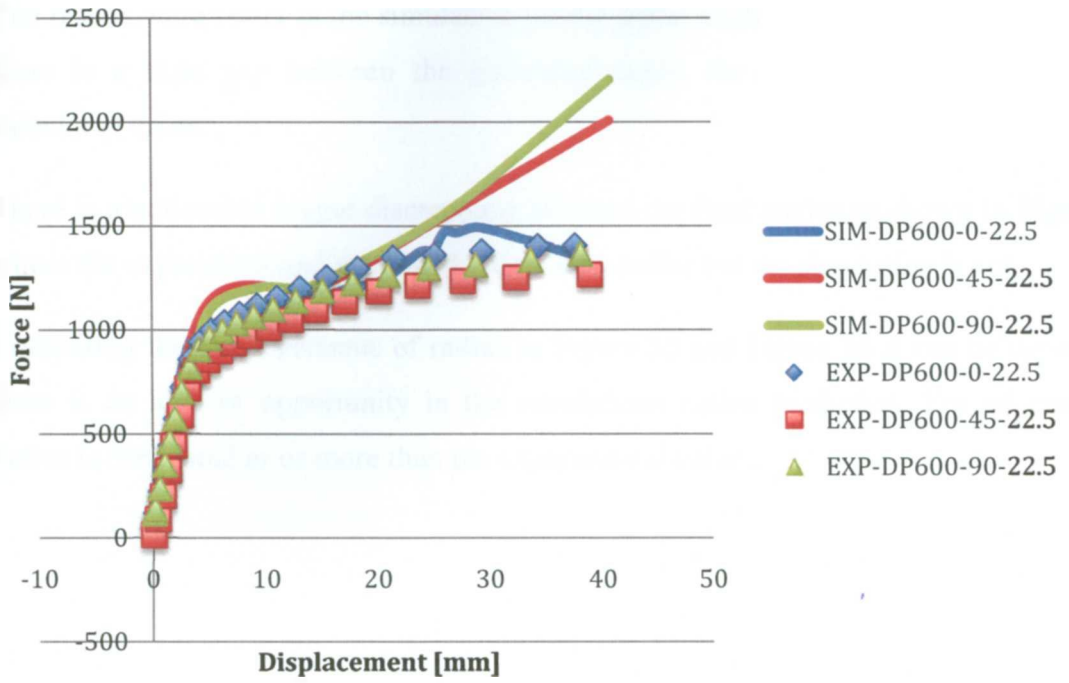

Figure 34. Force results for punch 22.5mm

The results were better in the simulation for the initial angle as shown in Figure 38 where there is a little gap between the simulated angle, the experimental and the CMM calculated value.

There is a noticeable bigger discrepancy between the final angles as shown in Figure 37, where the experiment and the CMM values are similar but the simulation is not.

Comparing the measurements of radius in Figure 35 and Figure 36 it can be shown that there is an area of opportunity in the simulations radius prediction. For all cases the radius is 30% smaller or more than the experimental value.

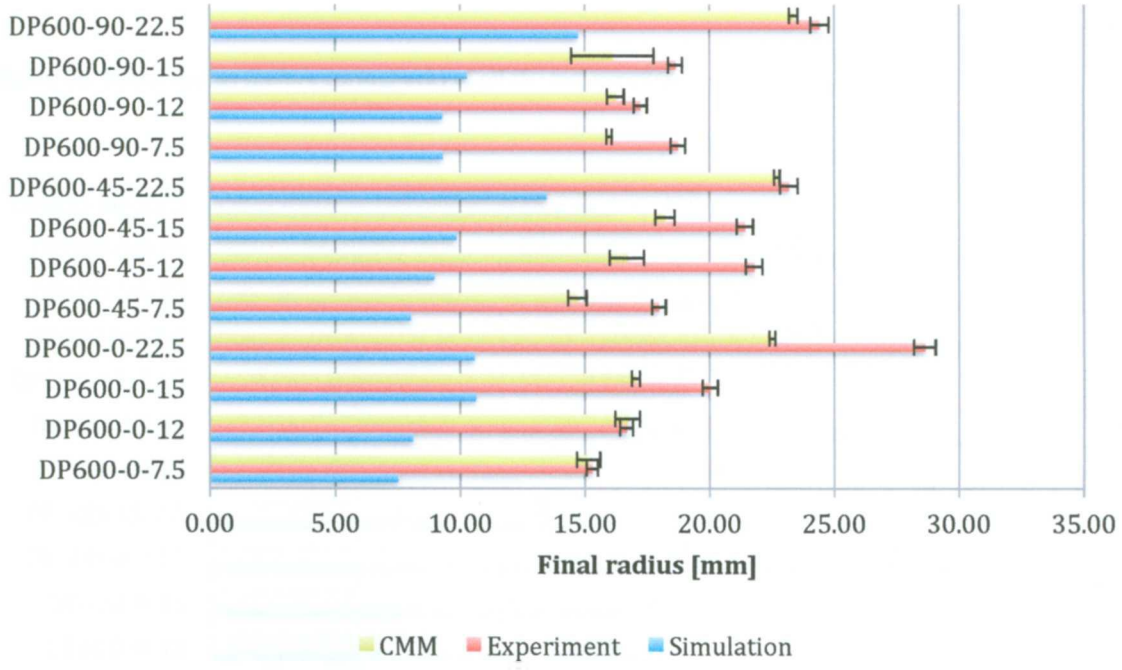

Figure 35. Final radius (after springback) of all the test samples

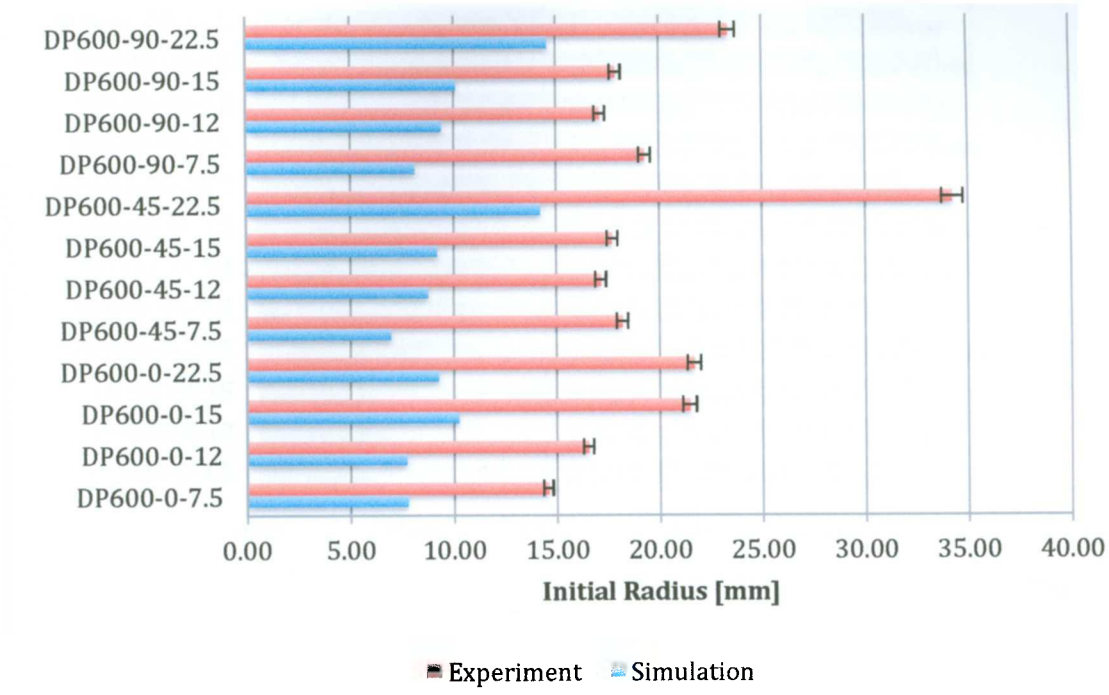

Figure 36. Initial radius (before springback) of all the test samples

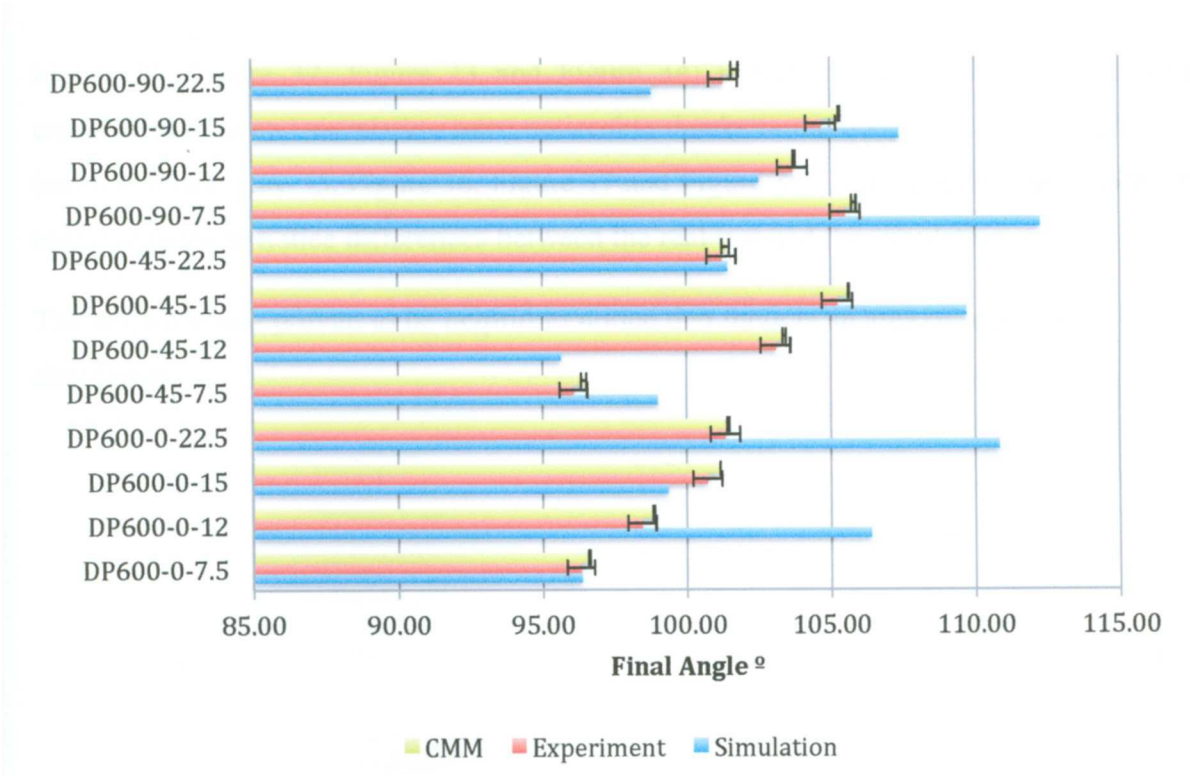

Figure 37. Final angle (after springback) of all the test samples

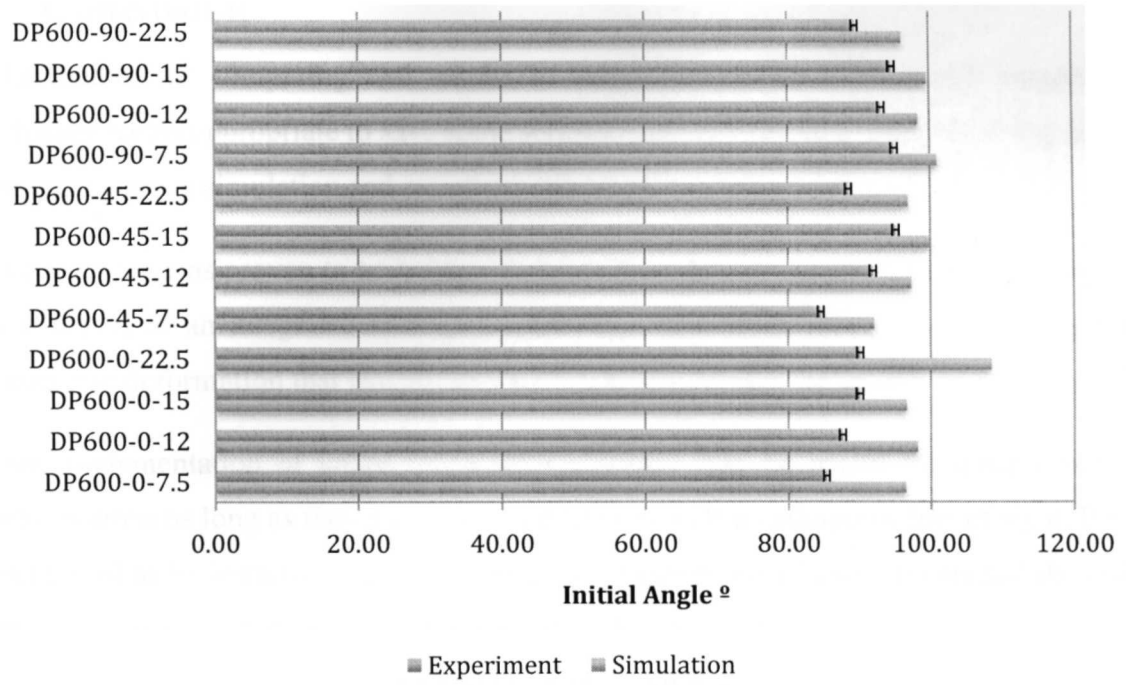

Figure 38. Initial angle (before springback) of all the test samples

The data acquired by the load cell may indicate that the simulation was fine (as shown in Figure 31, Figure 32, Figure 33 and Figure 34) however other differences between experimentation and simulation were noticeable thanks to the image recognition software (as shown in Figure 35, Figure 36, Figure 37 and Figure 38). It is an additional automatic tool that helps to notice differences between the real test and the simulation.

The software was proven to be helpful to notice that there is an area of opportunity in the simulation.

6 Conclusion

The method of comparing real results to simulation results with image recognition software seems appropriate to save some serious time. If integrated correctly it may lower the gap between simulation and experimentation.

The software was proven to be helpful to notice that there is an opportunity to implement it as a part of an integrated testing machine with simulation. There is a test related to strain-rate deformation that may be needed to achieve the desired results.

This implementation of image recognition software may be useful for other kinds of deformations as long as they are visible and there is a clear orthogonal line of sight. It's a useful tool to be implemented an automated for different visual experiments and the code can be tailored for the different simulations. A future for this code could be to interpret video so that it can assist on each step of the deformation, and be integrated into the hardware and software of specialized machines.

The CMM measurements depends on the expertise of the technician and the zones that he choses to measure. By measuring the middle of the curve the technician achieved less error on the different measurements but the software measures the whole curve, so even though the CMM is very accurate, said accuracy depends on the points taken and that's why there isn't a real way to measure it correctly.

The current programs for image measurement requires a continuous input from the user, which describes the circles, lines and overall desired geometry to measure over the digital image. This is very useful for many different applications, but for specialized measurements like the subject of this research it's not fast enough or reliable enough.

There is a promising future for implementing algorithms often used in other disciplines for mechanical purposes because they have been proven and implemented for years and can inject new life into current processes.

7 Works Cited

Chakrabarty, J. (2010). Applied Plasticity. FL: Springer.

Cheng-Bo, Y. (2009). Finger-vein image recognition combining modified hausdorff distance with minutiae feature matching. J. Biomedical Science and Engineering, 261-272.

Cheung, K. [. (2005). Getting started with Mathematica (Second ed.). NJ: Wiley.

Corona, J. G. (2010). Title pending. ITESM.

DEFORM. (n.d.). Deform V.10.1 Integrated System Manual.

Dunne, F. (2005). Introduction to Computational Plasticity. Oxford: Oxford University Press.

Dvorkin, E. (2006). Nonlinear Continua. NY: Springer.

Garcia-Romeu, M. L. (2005). Contribución al estudio del proceso de doblado al aire de chapa. Modelo de predicción del ángulo de recuperación y de radio de doblado final. Girona.

Gil Sevillano, J. (2003). Thin sheets-Anisotropy, formability & strain localization. San Sebastian: TECNUN.

González, R. C. (2009). Digital Image Processing using MATLAB. Gatesmark Publishing.

Hudgins, A. (2010). Predicting instability at die radii in advanced high strength steels. Colorado School of Mines, Advances Steel Processing and Products Research Center. CO: ELSEVIER.

IISI. (2006). Schematics of AHSS steels compared to low strength steels and traditional HSS.

Kalpakjian, S. (2003). Manufacturing Processes for Engineering Materials. NJ: Pearson Education.

Keler, S. (1994). Application and Forming of higher strength steel. J. Mater. Process.

Koppel Conway, A. (2009, 08). Advanced High Strength Steel. Retrieved 11 2010, from Collision Standard: http://www.collisionstandard.com/

Lin, J.-J. (2010). Pattern Recognition of Fabric Defects Using Case-Based Reasoning. Textile Research Journal .

Marciniak, Z. e. (2002). Mechanics of Sheet Metal Forming. Oxford: Butterworth-Heinemann.

Reza Fallahi, A. (2010). A new approach for classification of human brain CT images based on morphological operations. J. Biomedical Science and Engineering , 78-82.

Russ, J. (1995). The image processing handbook. Boca Raton: CRC Press.

Seber, G. A. (2003). Nonlinear Regression. NJ: Wiley.

Simo, J. (1998). Computational Inelasticity. NY: Springer.

Singuang Xu, K. Z. (2005). Springback Prediction, Compensation and Correlation for Automotive Stamping. Numisheet .

8 Appendix

8.1 Basic theory

8.1.1 Material properties

The most important criteria for selecting a material are related to qualities such as strength, stiffness, density, corrosion resistance and formability (for sheet metal materials). To assess formability we must describe the behavior in an exact way and thus we need to make the mechanical the required mechanical tests. (Marciniak, 2002)

Many familiar properties are based on measurements made in the tensile test. A tensile test-piece is shown in Figure 39. This is typical of a number of standard test-pieces having a parallel, reduced section for a length that is at least four times the width, w_0. The initial thickness is t_0 and the load on the specimen at any instant P , is measured by a load cell in the testing machine. In the middle of the specimen, a gauge length l_0 monitored by an extensometer and at any instant the current gauge length is l and the extension is $l = l - l0$.

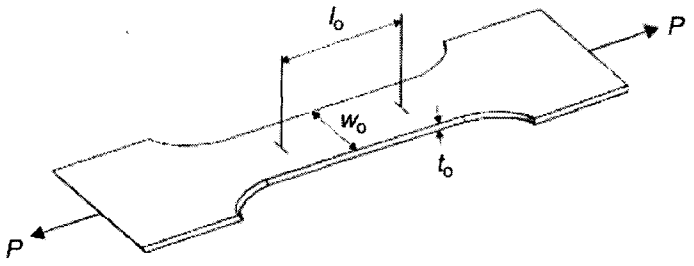

Figure 39. Typical test-piece (Marciniak, 2002)

During the test, load and extension will be recorded in a data acquisition system and a file created; this is then analyzed and various material property diagrams can be created. (Marciniak, 2002)

8.1.2 Elasto-plasticity

The spring back phenomenon is due to the elasto-plasticity of the material and the different states of elasticity or plasticity along the material's thickness.

To simulate an elastoplastic material the following ingredients are needed according to (Dvorkin, 2006)

1. A yield surface that in the 3D stress space describes the locus of the points where plastic behavior is initiated.
2. A flow rule that describes the evolution of the plastic deformations
3. A hardening law that describes de evolution of the yield surface during the plastic deformation process.

8.1.3 Spring-back

One of the most common metalworking operations is bending. This process is used not only to form parts such as flanges, curls, and corrugations, but also to impart stiffness to a part by increasing its moment of inertia (Kalpakjian, 2003).

The outer fibers of the part being bent are in tension, and the inner fibers are in compression. Because all materials have a finite modulus of elasticity, plastic deformation is followed by elastic recovery upon removal of the load; in bending, this recovery is known as spring-back (Kalpakjian, 2003).

Negative spring-back occurs when the bend angle in some cases becomes larger after the bend has been completed and the load is removed. This phenomenon is generally associated with V-die bending. This can be explained by observing the Figure 40 if the bent piece at stage (b) is removed, it will undergo positive spring-back. At stage (c), the ends of the piece are touching the male punch and are bent the other way so when it is released it can spring-back in the opposite direction, thus having negative spring-back. (Kalpakjian, 2003)

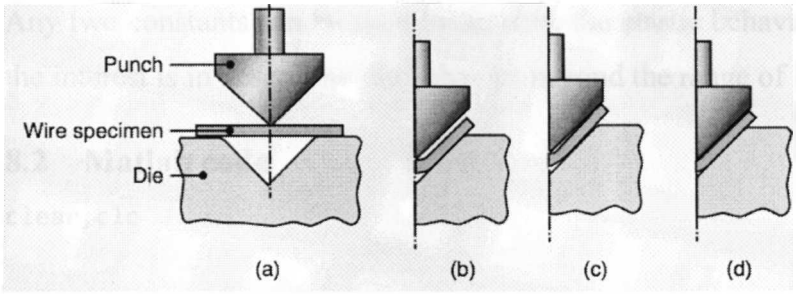

Figure 40. The particular case for negative springback (Kalpakjian, 2003)

8.1.4 Von Mises yield criterion

Because materials don't yield under hydrostatic conditions we need a prediction of when the material will Yield that is different enough from the hydrostatic stress. The yield condition of von Mises is used to describe the elastic limit. In the principal stress space, the yield condition can be written as Equation 4. (Dvorkin, 2006)

Equation 4

$$(\sigma_1^2 + \sigma_2^2 + \sigma_3^2) - \sigma_1\sigma_2 - \sigma_2\sigma_3 - \sigma_1\sigma_3 = 3k^2 = \sigma_y^2$$

This equation describes a Yield surface that in space is a cylinder in the direction (1,1,1) in that sense the hydrostatic stress does not produce Yield as shown in Figure 41.

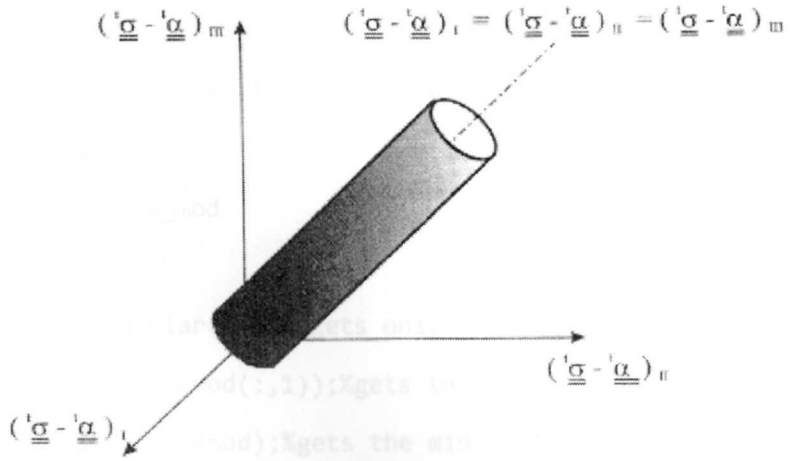

Figure 41. Yield Surface in 3D space (Dvorkin, 2006)

Any two constants can be used to describe the elastic behavior of a material. In this case the interest is in describing the behavior beyond the range of linear elasticity.

8.2 Matlab code

```
clear,clc


muestra=['A22.jpg'];
%list of test files ['sample1.jpg';'sample2.jpg']
[tam n]=size(muestra);
espesor=[3.01]; %sheet metal thickness [2;3]


for k=1:tam %for a sample size tam
tic%to take time t1
    root=imread(muestra(k,:));%gets k-th image
    t=espesor(k,:);%gest k-th thickness
    mod=limpiar(root);%calls a subroutine to get a binary image and clean
defects
   %limits the image width
    limwidth=800;
    [trash x_mod]=size(mod);
    if (x_mod >= limwidth)
    mod=imresize(mod,limwidth/x_mod);
    root=imresize(root,limwidth/x_mod);
    end;
    clear x_mod


    mod=aislar(mod);%gets only the biggest area
    t_pv=sum(mod(:,1));%gets the vertical thickness in pixels
    mod=media(mod);%gets the mid sufrace
    mod=borde(mod,t_pv);%crops image
t1=toc; %takes time t1
```

```
    figure(1);[trash c]=imcrop(mod);%ask the user to put the curve in a square
tic%takes time t2
    clear trash
    close Figure 1
    c=round(c);
    mod(c(2):c(2)+c(4),c(1):c(1)+c(3))=0;%removes a square section
    [L Ne]=bwlabel(mod);
    clear mod
    prop=regionprops(L,'Orientation');%gets the angle of both straight lines
    angs=sort([prop(1).Orientation prop(2).Orientation]);
    ang=180+angs(1)-angs(2);%gets the bend angle
    t_p=t_pv*cos(abs(angs(1))*pi/180);%converts vertical pixels to thickness
pixels
    pix2mm=t/t_p;
    %makes the image more symetric
    rot=-(angs(2)+angs(1))/2;
    mod=imrotate(root,rot,'bilinear');
    angs=angs+rot;
    mod=limpiar(mod);
    mod=aislar(mod);
    mod=mincrop(mod);
    mod=borde(mod,t_p);
    root=mod;
    %Non linear regresion for internal radius
    mod=sup(mod);%gets the top border
    mod=doblez(mod,angs,t_p);
    mod=aislar(mod);
    npi=nnz(mod);
    [rpi,Yi,Xi]=regresion(mod);%makes a non linear regression for a circle
    rpi=rpi-0.5;
```

```
    %Non linear regresion for exterior radius
    mod=root;
    mod=sub(mod);%gets the bottom border
    mod=doblez(mod,angs,t_p);
    mod=aislar(mod);
    npe=nnz(mod);
    [rpe,Ye,Xe]=regresion(mod);%makes a non linear regression for a circle
    rpe=rpe+0.5;
    npt=npe+npi;
    r_p=(rpe-t_p)*npe/npt+rpi*npi/npt;
    r=r_p*pix2mm;
t2=toc;
tiempo(k)=t1+t2;%gets the time for the k-th iteration
radio(k)=r;
angulo(k)=ang;
npix(k)=npi+npe;

    figure(2)%shows results
    m=ceil(sqrt(tam));
    subplot(m,m,k),
    plot(Xi,Yi+t_p,'.r',Xe,Ye,'.g');
    hold on
    plot(Xi,rad(rpi,Xi)+t_p,'-b',Xe,rad(rpe,Xe),'-b');
    title({muestra(k,:);['Angº= ' num2str(ang)];['Rad int= ' num2str(r,4)]});
    axis equal;
    hold off
end

function [img]=aislar(img)
%This functions isolates the biggest white area in a BW image
```

```
L=bwlabel(img);
propied=regionprops(L,'Area','BoundingBox');
Amax=max([propied.Area]);
s=find([propied.Area]<Amax);
for n=1:size(s,2)
d=round(propied(s(n)).BoundingBox);
img(d(2):d(2)+d(4),d(1):d(1)+d(3))=0;
end

function [img]=borde(img,t)

%deletes imperfections in the border
[y_img,x_img] = size(img);
img=imcrop(img,[t,0,x_img-2*t,y_img]);

function [img] = doblez(img,angs,t)
%gets only the bending zone

[m,n]=size(img);
    m1=find(img(:,1)==1);
    m2=find(img(:,n)==1);
    for x = 1:n%draws two straight lines
        rect(m1+round(x*tan(-angs(1)*pi/180)),x)=1;
        rect(m2+round((n-x)*tan(angs(2)*pi/180)),x)=1;
    end
    B=strel('disk',ceil(t/30));
    rect=imdilate(rect,B);
    rect=imcrop(rect,[0,0,n,m]);
    img=img&not(rect);%boolean operations to get only the bending zone
```

```
    img=mincrop(img);

function[img]=limpiar(img)
%This function converts the image to BW
img=rgb2gray(img);
umb=graythresh(img);
img=im2bw(img,umb);

function[img]=media(img)
%Makes a thin line
img=bwmorph(img,'thin',Inf);

function [img]=mincrop(img)
%removes border imperfections
c=minrect(img);
img=imcrop(img,c);

function [c]=minrect(img)
%get's the minimum coordinates for the image
[m,n]=find(img==1);
c=[min(n),min(m),range(n),range(m)];

function [y] = rad(r,x)
%Function for the circle for the lower quadrants
y=r-sqrt(r.^2-x.^2);

function [r_p,Y,X] = regresion( img )
%Gets the non linear regression for a circle
[Y X]=find(img==1);%get's the XY coordinates
Y=-Y;Y=Y-min(Y);%adjusts the Y values to start in 0
```

```
X=X-mean(X(find(Y==0)));%centers the X values
[r0,n]=size(X);
r_p=nlinfit(X,Y,@rad,r0);%makes the non linear regression


function[img]=sub(img)
%Gets the bottom border
B=[0,1,0;
    0,1,0;
    0,-1,0];
img=bwhitmiss(img,B);
```

8.3 Flow chart

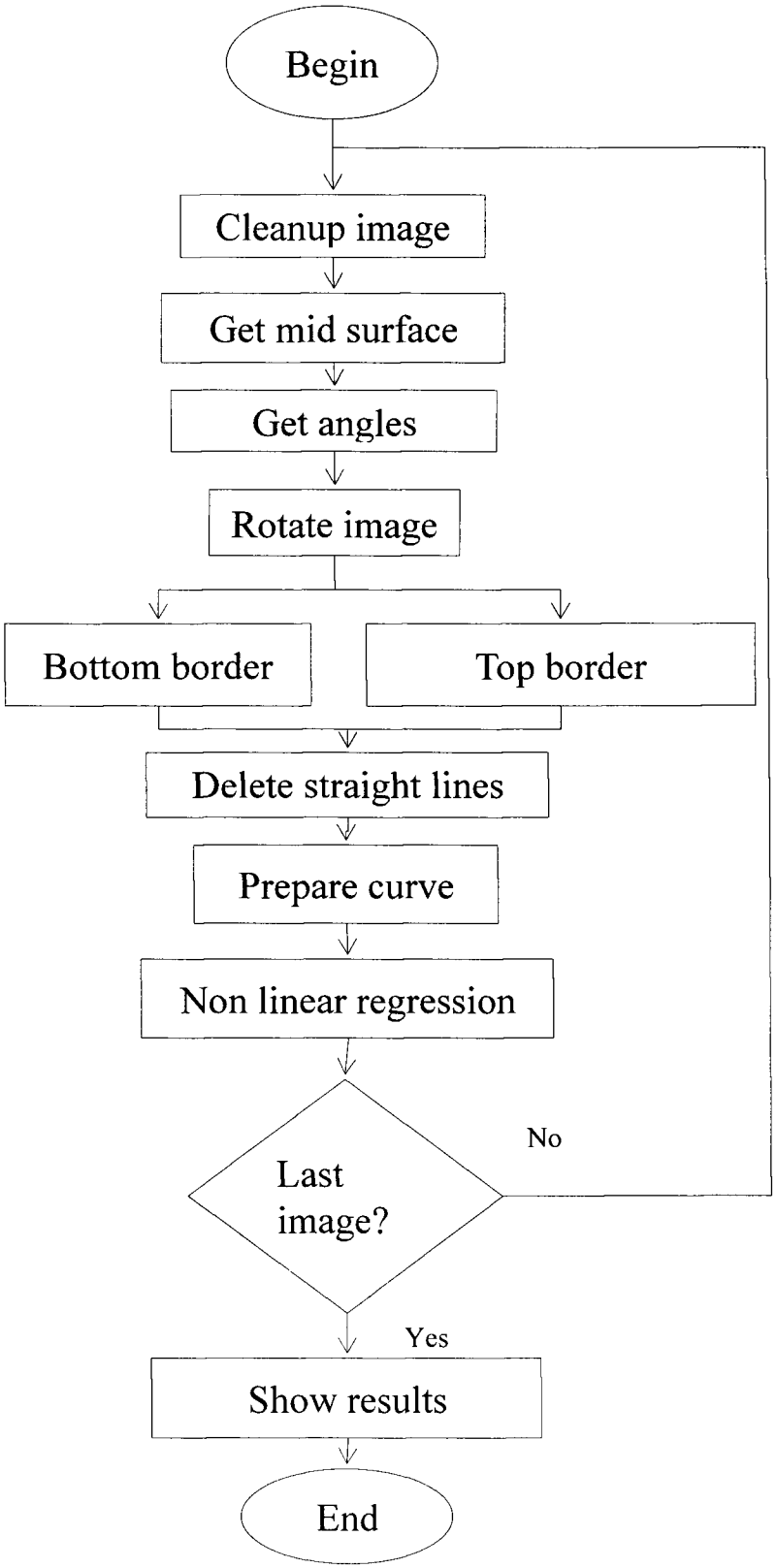

Figure 42. Flow chart for the image recognition algorithm

8.4 Recommendations

- The digital image method depend on the bending radius, an image with 1200px width is enough for the correct working of the algorithm.
- It is recommended to adjust the contrast and brightness previously to ensure there is a difference between the background and the sample piece and remove some imperfections.
- It is recommended to use a moderate compression for JPG files, around 80%
- The general format of the image must be like in Figure 43, where the red zone is the input image and the green zone is the bending zone.

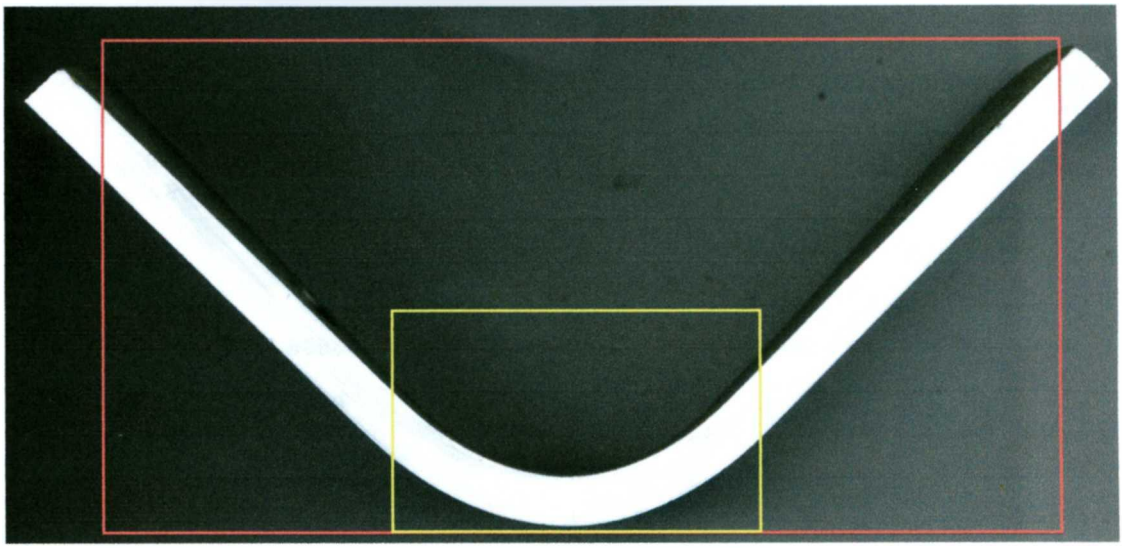

Figure 43. Recommended import file

- The green zone must separate one straight line from the other.

8.5 Deform .key file

```
*
*  DEFORM-3D V6.1 (Service Pack 1)   KEYWORD FILE (Qt)
*
*
*  Process Definition
*
TITLE
DEFORM SIMULATION
CURSIM       1       0       0
SIMNAM
OPERATION 1
SMODE        1
STYPE        1
MESHNO      25
UNIT         1
TNOW    0.0000000E+000  0.0000000E+000       0  0.0000000E+000
TRANS        0       1       0       0       0
HTMTHD       0
STNOUT       0       0       0       0       1       0       0
ELMNOD      10
       0       0       0       0       0       0       0       0       0
0
*
*  Stopping & Step Controls
*
NSTART      -1
STPINC       1
PDIE         2       0
NSTEP       25
```

```
EMAX    0.0000000E+000
TMAX    1.3000000E+000
SMAX    0.0000000E+000  0.0000000E+000  0.0000000E+000
VMIN    0.0000000E+000  0.0000000E+000  0.0000000E+000
LMAX    0.0000000E+000  0.0000000E+000  0.0000000E+000
STPDEF       1
DTMAX   5.0000000E-002  0.0000000E+000
DTTYPE       0       0
SLDERR  0.0000000E+000
DTPMAX  0.0000000E+000  0.0000000E+000  0.0000000E+000
DVMAX   0.0000000E+000  0.0000000E+000
MDSOBJ       0       0       0  0.0000000E+000
DTSUB   1.0000000E+000
DPLEN   5.0000000E-001
ODMAX   0.0000000E+000
*
*  Iteration Controls
*
CVGERR  5.0000000E-003  5.0000000E-002
ITRMTH       1
SOLMTD       1
ITRMXD     200
DEFBWD       1
SOLMTT       1
ITRMXT     200
TMPBWD       1
LATENT       0
*
*  Processing Conditions
*
```

```
GEOERR  1.0000000E-006  1.0000000E-004
PENINF  1.0000000E+009
UNTE2H  1.0000000E+000
TINTGF  7.5000000E-001
BLZMAN  5.6690000E-011
ENVTMP       0  2.0000000E+001
CNVCOF       0  2.0000000E-002
ENVMPR  1.2600000E-009
ENVMPT  8.8000000E-015
EHRATE  0.0000000E+000
ENVATM       0  1.6900000E+000
ACVCOF       0  2.5000000E-004
*
*  User Defined Variables
*
UNNAME       1       2


UENAME       1       2



*
*  Property Data of Material     2
*
MTNAME       2
DP600
FRAE2H       2  9.0000000E-001
FPERV        2  0.0000000E+000
FRCMOD          2          0   0.0000000E+000   0.0000000E+000   0.0000000E+000
0.0000000E+000
```

```
FSTRES       2       2

       3       2       1

  1.0000000E-003  5.0000000E-002  1.3000000E-001

  1.0000000E+000  1.0000000E+002

  2.1111111E+001

  3.9979000E+002       5.3600000E+002       6.1900000E+002       4.1300000E+002
5.4900000E+002

          6.3300000E+002

YOUNG        2       0  1.3525500E+005

POISON       2       0  3.0000000E-001

EXPAND       2       0  0.0000000E+000  2.0000000E+001

THRCND       2       1       3

  1.4900000E+002  1.8000000E+000

  8.7100000E+002  3.9000000E+000

  9.5810000E+002  3.9000000E+000

HEATCP       2       0  3.6000000E+000

EMSVTY       2       0  7.0000000E-001

HDNPHA       2       0  0.0000000E+000

MSTMTR       2       0

CREEP        2       0

DIFCOE       2       0  0.0000000E+000

ELRST        2       0  0.0000000E+000

UTSDAT       2       0  0.0000000E+000

HDNRUL       2       0

PMEAB        2       0  0.0000000E+000

PMITT        2       0  0.0000000E+000

MATDEN       2  0.0000000E+000

ANISO        2       2       3       1

       1

  0.0000000E+000  9.7000000E-001  9.9500000E-001  9.9400000E-001
```

```
BURGRS        2        0  0.0000000E+000

ALPHA         2        0  0.0000000E+000

NDISFM        2        0  0.0000000E+000

SRFNRG        2        0  0.0000000E+000

*

*  Inter-Material Data

*

*

*  Data for Object #     1

*

OBJTYP        1        5       0

OBJNAM        1

workpiece

AVGSTR        1  1.0000000E+000

LMTSTR        1  1.0000000E-002

PENVOL        1  1.0000000E+006

REFTMP        1  6.8000000E+001

TMPLMT        1  0.0000000E+000

ROTSYM        1  0.0000000E+000

  0.0000000E+000  0.0000000E+000  0.0000000E+000

  0.0000000E+000  0.0000000E+000  0.0000000E+000

TRGVOL        1        0  0.0000000E+000

ELPSOL        1        2

OTPRNG        1        0  0.0000000E+000  0.0000000E+000

PRSNAM        1


MOVCTL        1        1        0  0.0000000E+000  0.0000000E+000 -1.0000000E+000
0.0000000E+000

STROKE        1  0.0000000E+000  0.0000000E+000  0.0000000E+000

ANGMOV        1        1        0  0.0000000E+000
```

```
CNTRAX       1  0.0000000E+000  0.0000000E+000  5.0000000E+001  0.0000000E+000
0.0000000E+000  0.0000000E+000  0.0000000E+000

ANGMO2       1       1       0  0.0000000E+000

CNTRA2       1  0.0000000E+000  0.0000000E+000  5.0000000E+001  0.0000000E+000
0.0000000E+000  0.0000000E+000  0.0000000E+000

OBJUPD       1       0

RZ           1    1446



DRZ          1       0  0.0000000E+000

DRMESH       1       0  0.0000000E+000

BCCDEF       1      28       0



BCCDFN       1       0       0

URZ          1       0  0.0000000E+000

FRZ          1       0  0.0000000E+000

PRZ          1       0  0.0000000E+000

BCCTMP       1       0       0

BCCTFN       1       0       0

NDTMP        1       0  6.8000000E+001

NDHEAT       1       0  0.0000000E+000

NDFLUX       1       0  0.0000000E+000

USRNOD       1       0  0.0000000E+000       2

ELMCON       1    5306       4



MTLGRP       1       0       2

STRAIN       1       0  0.0000000E+000

STNCMP       1       0       6  0.0000000E+000

DENSTY       1       0  1.0000000E+000
```

```
DAMAGE        1        0  0.0000000E+000

STRESS        1        0  0.0000000E+000

YLDS          1        0  0.0000000E+000

USRELM        1        0  0.0000000E+000       2

RMDPTH        1  5.0000000E-001

RMSTRK        1  0.0000000E+000

RMTIME        1  0.0000000E+000

RMSTEP        1  0.0000000E+000

MGSIZR        1  5.0000000E+000

MGWTMP        1  0.0000000E+000

MGWSTN        1  1.6500000E-001

MGWSTR        1  1.6500000E-001

MGNELM        1    2000    8000    1000       0

MGTELM        1       4

MGWCUV        1  0.0000000E+000

MGGRID        1      25      25

MGERR         1  1.0000000E-002  3.2000000E+001

MGWUSR        1  1.0000000E+000  1.8813092E-001       1

MGUSER          1          1   1.8813092E+000   0.0000000E+000   0.0000000E+000
0.0000000E+000       1       1

       1 -2.6133484E+001 -7.8077301E+000  1.6112642E+001

       2  4.2464750E+001 -7.8077301E+000  1.6112642E+001

       3  4.2464750E+001  7.3484488E+000  1.6112642E+001

       4 -2.6133484E+001  7.3484488E+000  1.6112642E+001

       5 -2.6133484E+001 -7.8077301E+000  6.0827943E+001

       6  4.2464750E+001 -7.8077301E+000  6.0827943E+001

       7  4.2464750E+001  7.3484488E+000  6.0827943E+001

       8 -2.6133484E+001  7.3484488E+000  6.0827943E+001

FRCSTP        1       0

FRCNEL        1       0
```

```
FRCMTH       1       0

CRPTIM       1       0

DATOM        1       0  0.0000000E+000

HDNEST       1       0       0  0.0000000E+000  0.0000000E+000

HDNOBJ       1       0  0.0000000E+000

BCCCRB       1       0       0

CRBFLX       1       0  0.0000000E+000

VOTAGE       1       0  0.0000000E+000

BCCRHT       1       0       0

RHTFLX       1       0  0.0000000E+000

CSFREQ       1       0  0.0000000E+000

VOLCRG       1       0  0.0000000E+000

ZEFI         1       0  0.0000000E+000

ECCDEF       1       0       0

ECDEFN       1       0       0

ECPRES       1       0  0.0000000E+000

ECCTMP       1       0       0

ECTMFN       1       0       0

ECHFLX       1       0  0.0000000E+000

ECCATM       1       0       0

ECATFN       1       0       0

ECAFLX       1       0  0.0000000E+000

MATAXI       1       0       9  1.0000000E+000  0.0000000E+000  0.0000000E+000
0.0000000E+000  1.0000000E+000  0.0000000E+000  0.0000000E+000  0.0000000E+000
1.0000000E+000

*

*  Data for Object #     2

*

OBJTYP       2       1       0

OBJNAM       2

punch
```

```
AVGSTR       2  1.0000000E+000

LMTSTR       2  1.0000000E-002

PENVOL       2  1.0000000E+006

REFTMP       2  6.8000000E+001

TMPLMT       2  0.0000000E+000

ROTSYM       2  0.0000000E+000

  0.0000000E+000  0.0000000E+000  0.0000000E+000

  0.0000000E+000  0.0000000E+000  0.0000000E+000

TRGVOL       2       0  0.0000000E+000

ELPSOL       2       2

OTPRNG       2       0  0.0000000E+000  0.0000000E+000

PRSNAM       2


MOVCTL       2       1       2  0.0000000E+000  0.0000000E+000 -1.0000000E+000
4

  0.0000000E+000  5.1470000E+001

  1.0000000E+000  5.1470000E+001

  1.0100000E+000 -1.0000000E+002

  1.2000000E+000 -1.0000000E+002

STROKE       2  0.0000000E+000  0.0000000E+000  0.0000000E+000

ANGMOV       2       1       0  0.0000000E+000

CNTRAX       2  0.0000000E+000  0.0000000E+000  9.4996830E+000  0.0000000E+000
0.0000000E+000  0.0000000E+000  0.0000000E+000

ANGMO2       2       1       0  0.0000000E+000

CNTRA2       2  0.0000000E+000  0.0000000E+000  9.4996830E+000  0.0000000E+000
0.0000000E+000  0.0000000E+000  0.0000000E+000

OBJUPD       2       0

DIEGEO       2       1      74     144



RMDPTH       2  5.0000000E-001
```

```
RMSTRK       2  0.0000000E+000
RMTIME       2  0.0000000E+000
RMSTEP       2  0.0000000E+000
MGSIZR       2  2.0000000E+000
MGWTMP       2  0.0000000E+000
MGWSTN       2  2.5000000E-001
MGWSTR       2  2.5000000E-001
MGNELM       2    2000    8000    1000       0
MGTELM       2       4
MGWCUV       2  5.0000000E-001
MGGRID       2      25      25
MGERR        2  1.0000000E-002  3.2000000E+001
MGWUSR       2  0.0000000E+000  1.0000000E+000       1
FRCSTP       2       0
FRCNEL       2       0
FRCMTH       2       0
CRPTIM       2       0
HDNEST       2       0       0  0.0000000E+000  0.0000000E+000
CSFREQ       2       0  0.0000000E+000
VOLCRG       2       0  0.0000000E+000
*
*  Data for Object #     3
*
OBJTYP       3       1       0
OBJNAM       3
base
AVGSTR       3  1.0000000E+000
LMTSTR       3  1.0000000E-002
PENVOL       3  1.0000000E+006
REFTMP       3  6.8000000E+001
```

```
TMPLMT        3  0.0000000E+000

ROTSYM        3  0.0000000E+000

  0.0000000E+000  0.0000000E+000  0.0000000E+000

  0.0000000E+000  0.0000000E+000  0.0000000E+000

TRGVOL        3        0  0.0000000E+000

ELPSOL        3        2

OTPRNG        3        0  0.0000000E+000  0.0000000E+000

PRSNAM        3


MOVCTL        3        1        0  0.0000000E+000  0.0000000E+000 -1.0000000E+000
0.0000000E+000

STROKE        3  0.0000000E+000  0.0000000E+000  0.0000000E+000

ANGMOV        3        1        0  0.0000000E+000

CNTRAX        3  0.0000000E+000  0.0000000E+000  0.0000000E+000  0.0000000E+000
0.0000000E+000  0.0000000E+000  0.0000000E+000

ANGMO2        3        1        0  0.0000000E+000

CNTRA2        3  0.0000000E+000  0.0000000E+000  0.0000000E+000  0.0000000E+000
0.0000000E+000  0.0000000E+000  0.0000000E+000

OBJUPD        3        0

DIEGEO        3        1     168     332



RMDPTH        3  5.0000000E-001

RMSTRK        3  0.0000000E+000

RMTIME        3  0.0000000E+000

RMSTEP        3  0.0000000E+000

MGSIZR        3  2.0000000E+000

MGWTMP        3  0.0000000E+000

MGWSTN        3  2.5000000E-001

MGWSTR        3  2.5000000E-001

MGNELM        3    2000    8000    1000       0
```

```
MGTELM       3       4
MGWCUV       3  5.0000000E-001
MGGRID       3      25      25
MGERR        3  1.0000000E-002  3.2000000E+001
MGWUSR       3  0.0000000E+000  1.0000000E+000       1
FRCSTP       3       0
FRCNEL       3       0
FRCMTH       3       0
CRPTIM       3       0
HDNEST       3       0       0  0.0000000E+000  0.0000000E+000
CSFREQ       3       0  0.0000000E+000
VOLCRG       3       0  0.0000000E+000
*
*  Inter-Object Data
*
CNTACT       1       2       1
FRCFAC       1       2       1       0  1.2000000E-001
IHTCOF       1       2       0  0.0000000E+000
SEPRES       1       2       0  0.0000000E+000
INTRST       1       2       0  0.0000000E+000
CNTMTH       1       2       0
CNTACT       1       3       1
FRCFAC       1       3       1       0  1.2000000E-001
IHTCOF       1       3       0  0.0000000E+000
SEPRES       1       3       0  0.0000000E+000
INTRST       1       3       0  0.0000000E+000
CNTMTH       1       3       0
```